

E3AD: An Emotion-Aware Vision-Language-Action Model for Human-Centric End-to-End Autonomous Driving

Yihong Tang¹, Haicheng Liao², Tong Nie³, Junlin He³, Ao Qu⁴, Kehua Chen⁵, Wei Ma³, Zhenning Li², Lijun Sun¹, Chengzhong Xu²

¹McGill University, ²University of Macau, ³The Hong Kong Polytechnic University,

⁴Massachusetts Institute of Technology, ⁵University of Washington

 Equal Contribution,  Corresponding Authors

Abstract

End-to-end autonomous driving (AD) systems increasingly adopt vision-language-action (VLA) models, yet they typically ignore the passenger’s emotional state, which is central to comfort and AD acceptance. We introduce Open-Domain End-to-End (OD-E2E) autonomous driving, where an autonomous vehicle (AV) must interpret free-form natural-language commands, infer the emotion, and plan a physically feasible trajectory. We propose E3AD, an emotion-aware VLA framework that augments semantic understanding with two cognitively inspired components: a continuous Valence-Arousal-Dominance (VAD) emotion model that captures tone and urgency from language, and a dual-pathway spatial reasoning module that fuses egocentric and allocentric views for human-like spatial cognition. A consistency-oriented training scheme, combining modality pretraining with preference-based alignment, further enforces coherence between emotional intent and driving actions. Across real-world datasets, E3AD improves visual grounding and waypoint planning and achieves state-of-the-art (SOTA) VAD correlation for emotion estimation. These results show that injecting emotion into VLA-style driving yields more human-aligned grounding, planning, and human-centric feedback.

Date: December 5, 2025

1. Introduction

Autonomous driving (AD) has evolved from modular pipelines to vision-language-action end-to-end (E2E) systems that directly map sensor inputs to vehicle controls through unified optimization. This paradigm significantly improves efficiency and adaptability by integrating perception, prediction, and planning into a single learning framework [6, 32]. Despite these advances, a fundamental obstacle remains that is not purely technical but human-centered: ensuring public trust and acceptance of fully autonomous driving [78].

While current E2E systems [22, 23, 48] exhibit strong control and perception capabilities, passengers often feel uneasy about delegating decisions to opaque algorithms that operate without acknowledging human intent or emotion. Surveys [74, 75] and behavioral studies [7, 36, 72] consistently indicate that emotional interaction is a critical determinant of user comfort and perceived safety. However, most existing models [29, 31, 46, 61] are designed for closed-loop rational control and remain insensitive to emotion cues such as anxiety or urgency. This disconnection between compu-

tational reasoning and emotional understanding forms what can be described as an *emotion gap* for autonomous vehicles (AVs). Bridging this gap requires reconsidering the role of human-vehicle interaction in AD. An intelligent system should understand “*what*” a passenger says and “*how*” it is expressed. For instance, the tone difference between “stop here” and “stop here now!” carries implicit emotional meaning that influences how the vehicle should respond. Recognizing such differences enables the system to regulate behavior that aligns with the passenger’s emotional state, providing reassurance and enhancing acceptance [25].

As illustrated in Fig. 1, we extend the conventional E2E AD framework toward a more human-centric paradigm. Future AVs must reason not only over visual and spatial cues but also interpret and respond to natural-language commands that convey the passenger’s intent and emotional state. We define this capability as the task of **Open-Domain End-to-End AD (OD-E2E)**, where the driving agent jointly reasons over semantic content, emotion context, and spatial environment to generate physically realizable trajectories consistent with the passenger’s instructions. This formulation moves

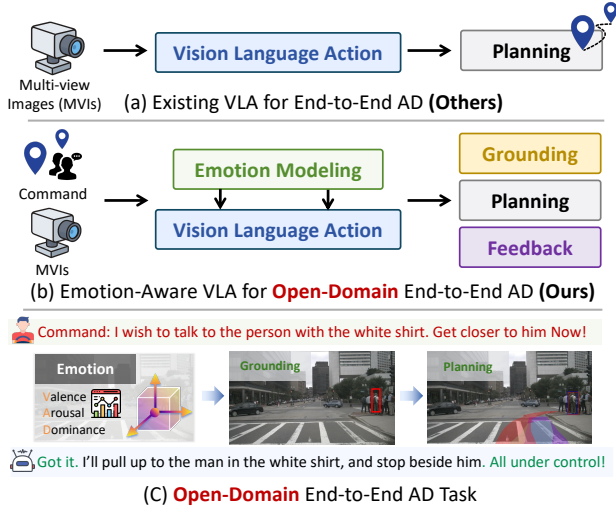


Figure 1. Overview of our proposed E3AD framework, contrasted with conventional VLA pipelines. (a) Existing VLA models behave as emotion-agnostic systems, mapping multi-view images directly to a planning output without human-in-the-loop interaction or emotion understanding. (b) Our model adds explicit emotion modeling and closed-loop feedback, allowing the agent to infer intent intensity, ground referents more reliably, and adapt its plan accordingly. (c) This yields the Open-Domain E2E AD task, where the agent jointly reasons over language, emotion, perception, and navigation to enable human-centered and context-aware autonomy.

beyond purely reactive control toward interactive, emotion-aware driving assistants that better match human expectations and preferences, transforming AVs from passive executors into empathetic and user-aligned driving agents [32].

Technically, our approach builds on the emerging Vision-Language-Action (VLA) paradigm [53], which unifies perception, reasoning, and control through large-scale multimodal modeling. By coupling visual and linguistic representations, VLA frameworks enable agents to perform complex goal-driven behaviors with improved generalization, interpretability, and alignment to human intent. Following this paradigm, we propose an **Emotion-aware End-to-End Autonomous Driving** framework, **E3AD**, which extends VLA from purely semantic understanding to emotion and spatially consistent reasoning. To enhance cognitive capability, E3AD incorporates two key components within a unified pipeline: (1) **Emotion Modeling**, which maps commands into a continuous Valence-Arousal-Dominance (VAD) space [17] to interpret emotional tone and behavioral urgency; and (2) **Spatial Reasoning**, which fuses egocentric and allocentric pathways to achieve human-like spatial cognition. These components are jointly optimized through a consistency-oriented learning strategy that enforces coherence between the semantic and emotional context of the command and the resulting trajectory. This design enables E3AD to reason jointly over *what* the passenger intends and *how* it is

expressed, producing emotion-aware and human-aligned driving behaviors in a fully E2E manner. From a safety perspective, modulating behavior according to passenger state decouples request satisfaction from the safety envelope, which is essential for calibrated trust in E2E AD.

Overall, the contributions of this study are threefold:

- We define Open-Domain End-to-End AD for human-centric AVs, which unifies semantic, emotional, and spatial reasoning from natural-language commands.
- We propose E3AD, an emotion-aware VLA framework that integrates continuous emotion modeling and dual-system spatial reasoning in a unified E2E pipeline, enabling emotion-grounded response and planning.
- We show that E3AD outperforms strong baselines on visual grounding, emotion estimation, and waypoint planning across multiple benchmarks, with particularly large gains on emotion-sensitive and corner-case scenarios.

2. Related Work

VLA for End-to-end AD. Recent work explores VLA architectures that inject world knowledge and reasoning from large multimodal models into E2E AD [9]. Existing approaches can be broadly grouped into three paradigms [25]. The first paradigm, represented by DriveGPT-4 [67], OpenEMMA [66], and CoT-Drive [35], produces scene-level explanations via QA-style prompts. While improving interpretability, they act as “commentators”, lacking precise spatial grounding and direct control fidelity. The second paradigm, such as Senna [24], VLP [47], and LMDrive [54], employs VLMs to generate discrete “meta-behaviors” to guide a low-level controller. This approach provides only sparse guidance that limits its capacity for continuous spatial reasoning, resulting in marginal gains in driving performance. The third paradigm, like Simlingo [50], AutoVLA [81], and FSDrive [73], couples VLM-based perception with dedicated planning modules that directly output trajectories or control signals, achieving strong performance. However, current VLAs [30, 37, 80] face two core issues: weak spatial understanding, operating largely in 2D without explicit 3D or allocentric (map-based) reasoning [58, 59], and a purely rational sequence-prediction view that ignores passenger emotion, crucial for intent and behavior alignment [57]. Building on the third paradigm, we propose an emotion-aware, spatially grounded end-to-end VLA.

Emotion Computing in AD. Emotional interaction between humans and AVs offers a promising path to improving public acceptance, safety, and comfort in AD [28]. However, enabling AVs to accurately perceive, interpret, and respond to human emotions remains a fundamental challenge [55, 56]. Early work [8, 45] emphasized driver-state monitoring (fatigue, distraction, stress) via physiological signals (EEG/ECG [5]) and visual cues (facial expressions [65] or gaze tracking); with higher-level AD, the focus shifted to

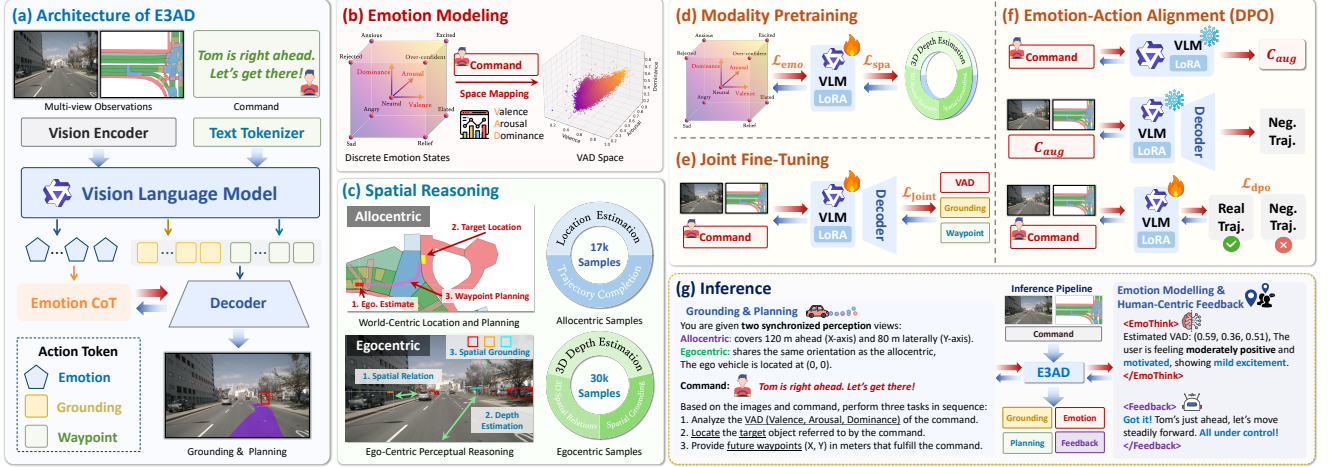


Figure 2. Overview of E3AD and its training/inference pipeline. Given egocentric and allocentric views with a natural-language command (a), E3AD outputs emotion, grounding, and waypoint tokens via two core modules: Emotion Modeling (b) encodes commands in continuous VAD space (c), and Spatial Reasoning fuses egocentric and allocentric pathway cues. Training proceeds from Modality Pretraining for emotion/spatial skills (d) to Joint Fine-Tuning that predicts $(\hat{e}, \hat{b}, \hat{\tau})$ in a single autoregressive chain (e), followed by Emotion-Action Alignment (f). During inference (g), E3AD runs end-to-end to estimate (\hat{e}) , ground (\hat{b}) , and plan $(\hat{\tau})$, producing human-centric feedback.

passenger experience (e.g., ride comfort [33, 34], anxiety [27, 64]). Most approaches, however, perform passive detection with discrete labels and decouple emotion estimation from downstream control. We instead ground emotion in the continuous VAD space, integrating it into a unified VLA. To our knowledge, E3AD is the first framework to use a VAD vector to simultaneously guide: (1) ambiguity resolution for nuanced language commands, and (2) the generation of downstream planning trajectories. Through consistency-oriented fine-tuning, E3AD aligns emotion with driving behavior, advancing from passive emotion recognition to a human-centric autonomous driving system [71].

3. Methodology

3.1. Problem Formulation

We consider OD-E2E AD, where an autonomous vehicle receives multi-view observations and a natural-language command and must execute the command through spatial grounding and motion planning. Let C denote the passenger’s command and $I = \{I_{\text{ego}}, I_{\text{allo}}\}$ denote the multi-view observations containing egocentric and allocentric views of the scene. The agent must (i) localize the object or location referenced in C and (ii) generate a physically feasible trajectory that fulfills the instructed intent. Formally, given the tuple (I, C) , the task aims to learn a mapping:

$$f_{\theta} : (I, C) \rightarrow \hat{\mathcal{Y}} = \{\hat{b}, \hat{\tau}\}, \quad (1)$$

where \hat{b} denotes the grounded target in the scene and $\hat{\tau} = \{y_t\}_{t=1}^T$ denotes the future waypoints. Unlike prior language grounding setups that restrict command vocabularies and

decouple referent localization from motion planning into separate modules, the OD-E2E task learns a single policy f_{θ} that, under a unified objective, jointly predicts $(\hat{b}, \hat{\tau})$ conditioned on (I, C) . This elevates language grounding from an auxiliary perception task to an integral component of the end-to-end decision-making objective.

3.2. Overview

Fig. 2 illustrates the overall architecture of E3AD, a cognitively inspired VLA system built on Qwen2.5-VL-7B-Instruct [1] that integrates Emotion Modeling, Two-System Spatial Representation, and Consistency-Oriented Action Planning in a unified pipeline. To strengthen its cognitive competence, we adopt a three-stage training strategy: (i) Foundational Modality Pretraining to establish emotion and spatial priors, (ii) Joint Reasoning Fine-tuning to optimize end-to-end multimodal operation, and (iii) Emotion-Action Alignment to ensure planning behaviors remain consistent with emotional intent. This progressive design provides fine-grained emotion understanding, cognitively grounded spatial reasoning, and behaviorally consistent planning, all aligned with the passenger’s semantic and emotional intent.

3.3. Emotion Modeling

Human-vehicle interaction in AD inherently involves emotional communication, yet most existing systems are emotion-agnostic and model affect, if at all, with a small set of discrete labels such as happy, angry, or sad [34]. Such coarse encoding cannot capture small but behaviorally meaningful changes in tone that influence how a command should be executed. We therefore adopt a continuous representation based

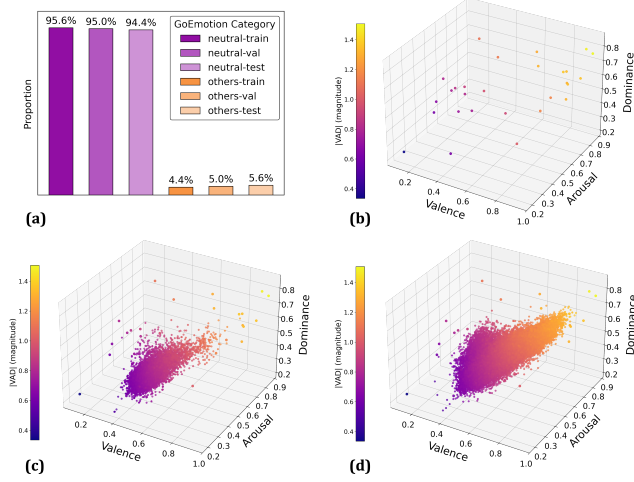


Figure 3. Visualization of emotion distributions before and after augmentation. (a) Proportions of GoEmotion categories across Talk2Car splits. (b) VAD distribution of GoEmotion. (c) Incorporating driving commands enriches emotional diversity. (d) Emotion-aware augmentation expands and smooths the VAD distribution, providing broader and continuous emotion supervision.

on the Valence-Arousal-Dominance (VAD) model [63], representing emotion as $e \in \mathbb{R}^3$. Valence measures positivity, arousal measures activation, and dominance measures control; in driving contexts, these axes correspond to attitude (calm vs. anxious), alertness (fatigued vs. vigilant), and control (confident vs. overwhelmed) [42].

To supervise this space, we derive VAD labels from both sentence-level and word-level cues. For each command C , we first apply the GoEmotions classifier [11] to obtain a distribution over discrete emotions and map it to sentence-level VAD scores using the label-VAD dictionary in [63]. In parallel, we compute a word-level VAD vector by removing stop words and averaging lexical scores over the remaining tokens. The final label e is obtained by combining these two sources, so that both global interpretation and emotion-bearing phrases are reflected (details in Appendix A.1).

Driving commands, however, are often emotionally neutral, which would encourage the model to ignore emotion if trained naively. To break this bias and disentangle intent from tone, we introduce emotion-aware command augmentation. For each command $C^{(i)}$, Qwen2.5-VL generates K paraphrases $C_{\text{aug}}^{(i)} = \{C_1^{(i)}, \dots, C_K^{(i)}\}$ that preserve the driving goal while varying the attitude or intensity. Each augmented command $C_k^{(i)}$ is assigned a VAD label $e_k^{(i)}$ via the same mapping procedure, forming an augmented set \mathcal{C}^* that creates neighborhoods of semantically equivalent but affectively distinct commands (Fig. 3). This forces the model to attribute changes in e to changes in tone rather than intent.

We then perform supervised fine-tuning (SFT) to equip the VLM with explicit emotion understanding. Given aug-

mented command-emotion pairs $\{(C_k^{(i)}, e_k^{(i)})\} \subset \mathcal{C}^*$, we cast emotion prediction as conditional generation with an instruction template (Appendix E) and define the loss as

$$\mathcal{L}_{\text{emo}} = -\mathbb{E}_{(C_k^{(i)}, e_k^{(i)}) \sim \mathcal{C}^*} [\log p_{\theta}(e_k^{(i)} | C_k^{(i)})], \quad (2)$$

where p_{θ} denotes the model’s distribution over quantized VAD tokens. Rather than adding a separate sentiment head, this continuous, instruction-style formulation embeds e into the same generative reasoning process as other outputs, enabling E3AD to represent fine-grained shifts in affect while keeping the underlying driving intent fixed and later conditioning planning behavior directly on the inferred emotion.

3.4. Spatial Reasoning

Inspired by the dual-system model of human spatial perception [2], we design the VLA backbone to reason over two complementary spatial pathways: an *egocentric* frame for immediate, action-oriented perception and an *allocentric* frame for global, map-based structure. This design compels the model to fuse local sensory cues with world-centered priors, mirroring how humans combine first-person observations with internal cognitive maps for reliable navigation.

Egocentric Pathway. The egocentric pathway captures the agent’s first-person perceptual field. Using annotated data samples, the model predicts (i) the relative 3D direction to the referent, (ii) its distance, and (iii) its grounded location in image coordinates from (I_{ego}, C) . These auxiliary signals provide fine-grained, short-horizon spatial cues essential for immediate control. We curate a dataset of 30K samples to establish a robust foundation for egocentric spatial reasoning, which directly supports subsequent planning.

Allocentric Pathway. The allocentric pathway encodes a world-centered representation akin to a cognitive map. Given BEV input I_{allo} , the model learns to (i) predict the target location in BEV coordinates and (ii) generate a coarse trajectory $\tau = \{y_t\}_{t=1}^T$ from the ego pose to that target. This supervision yields long-horizon spatial structure, road topology, occlusions, and multi-agent layout, producing map-consistent priors that complement egocentric perception. We use roughly 17K samples to teach this world-centered reasoning. In combination, the two pathways supply complementary local and global spatial cues that downstream planning modules can exploit for grounding and trajectory waypoint generation in cluttered, partially observed scenes.

3.5. Action and Feedback

Action Decoder. Following the VLA backbone, we append a lightweight action decoder f_{act} that is responsible for translating the VLA’s high-level outputs into a precise, physically-realizable trajectory $\hat{\tau}$. Conditioned on the grounded target \hat{b} , the coarse trajectory $\tilde{\tau}$, and visual observations I , the decoder outputs the final trajectory $\hat{\tau} = f_{\text{act}}(\hat{b}, \tilde{\tau}, I)$, where $\hat{\tau} \in \mathbb{R}^{T \times 2}$ represents the coordinates of planned waypoints.

Human-centric Verbal Feedback. To mitigate passengers’ “black-box” anxiety, E3AD provides verbal feedback \hat{r} after planning the waypoints. We employ the trained Qwen2.5-VL backbone to generate this response. Specifically, the model is guided by structured prompts, conditioning the generation of \hat{r} on the complete output of the VLA pipeline: the predicted emotion state \hat{e} , the grounded target \hat{b} , and the planned waypoints $\hat{\tau}$. The feedback policy adapts tone, length, and specificity to emotion and urgency: for calm states, it offers brief confirmations, whereas for high arousal, it produces direct, time-critical guidance. This verbal feedback loop improves transparency and user trust by aligning language, planned motion, and passenger emotion, transforming the AV from an opaque tool into a human-centric agent.

3.6. Consistency-Oriented Training and Inference

We adopt a three-stage consistency-driven training strategy to progressively endow E3AD with emotion awareness, spatial reasoning, and coherent decision-making. The training stages consist of: (1) Modality Pretraining, which establishes foundational representations for spatial and emotional cues; (2) Joint Fine-tuning, unifying emotion grounding, scene understanding, and trajectory planning within a single autoregressive generation process; and (3) Emotion-Action Alignment, designed for stable, emotion-consistent driving behaviors. Each training stage is elaborated as follows:

Stage-1: Modality Pretraining. In this initial stage, we apply supervised fine-tuning to equip E3AD with spatial and emotion perception skills separately: (1) Emotion Modeling is trained on our augmented command dataset \mathcal{C}^* using the emotion regression loss \mathcal{L}_{emo} . (2) Spatial Reasoning is trained on our synthetic egocentric and allocentric pathways using the negative log-likelihood loss $\mathcal{L}_{\text{spatial}}$ of next-token prediction to optimize spatial reasoning across both views.

Stage-2: Joint Fine-Tuning. After modality pretraining, we fine-tune the VLA to unify these capabilities into a single, coherent reasoning process. We employ an instruction-based SFT paradigm where the model autoregressively predicts the full output sequence $\mathcal{T} = (\hat{e}, \hat{b}, \hat{\tau})$ in a single forward pass. This joint objective $\mathcal{L}_{\text{joint}}$ is formally defined as follows:

$$\mathcal{L}_{\text{Joint}} = -\mathbb{E}_{(I, C, \mathcal{T})} \sum_{t=1}^{|\mathcal{T}|} \log p_{\theta}(\mathcal{T}_t \mid \mathcal{T}_{<t}, I, C), \quad (3)$$

where p_{θ} is the conditional token distribution. This encourages the VLA to form an emotion-aware chain of thought, where the predicted emotion \hat{e} and spatial grounding \hat{b} directly inform the subsequent generation of waypoints $\hat{\tau}$.

Stage-3: Emotion-Action Alignment (DPO). While $\mathcal{L}_{\text{Joint}}$ aligns tasks, it does not explicitly enforce behavioral consistency with different emotional intent. Standard preference-based alignment methods (like DPO) are non-trivial to apply in this field, as AD datasets typically provide only a single,

optimal ground-truth trajectory $\tau^{(i)}$ for any given command $C^{(i)}$, rather than ranked preference pairs. To address this, we construct a dataset of *pseudo-preference pairs* via emotion-augmented commands. For each original command $C^{(i)}$ and its ground-truth trajectory $\tau^{(i)}$, we identify an emotion-augmented variant $C_{k-}^{(i)}$ whose VAD embedding deviates most from the original. We use this “negative” command to generate a dispreferred, emotion-shifted trajectory $\tilde{\tau}_{k-}^{(i)}$:

$$C_{k-}^{(i)} = \arg \max_k \|e_k^{(i)} - e^{(i)}\|_2, \tilde{\tau}_{k-}^{(i)} \sim p_{\theta}(\tau \mid C_{k-}^{(i)}, I^{(i)}), \quad (4)$$

This yields a preference pair $(\tau^{(i)} \succ \tilde{\tau}_{k-}^{(i)})$ for the command $C^{(i)}$. We apply DPO [49] to optimize this preference:

$$\mathcal{L}_{\text{dpo}} = -\mathbb{E}_i \left[\log \sigma \left(\beta \left(\log p_{\theta}(\tau^{(i)} \mid C^{(i)}) - \log p_{\theta}(\tilde{\tau}_{k-}^{(i)} \mid C^{(i)}) \right) \right) \right]. \quad (5)$$

Notably, this stage encourages the model to assign higher likelihood to trajectories consistent with the original command’s intent while suppressing emotionally perturbed alternatives, leading to stable yet emotion-aware behavior.

Inference. After the VLA backbone is trained, its outputs are integrated into a lightweight action decoder for precise trajectory waypoint generation. During inference, E3AD operates end-to-end: it seamlessly processes the input tuple $(I_{\text{ego}}, I_{\text{allo}}, C)$ to directly produce the emotion state \hat{e} , the grounded target \hat{b} , coarse trajectory waypoints $\hat{\tau}$, and the verbal response \hat{r} for passengers. This integrated process enables emotion-grounded visual grounding and human-aligned planning without additional post-processing.

4. Experiments

4.1. Experiment Setups

Datasets. This study conducts experiments on several challenging real-world benchmarks, including Talk2Car [18], DrivePilot [19], MoCAD [34], and Talk2Car-Trajectory [15]. To further assess model robustness, we follow the ThinkDeeper protocol [19] and introduce refined data splits for the DrivePilot and MoCAD, resulting in two tailored subsets: Long-Text and Corner-Case, each presenting distinct challenges.

Evaluation Metrics. We evaluate models along two axes: (1) joint end-to-end performance and (2) sub-task ablations. For end-to-end evaluation, we report trajectory metrics, including ADE, FDE, Fréchet, DTW, SSPD, and planning accuracy within g meters (PA_g). For sub-task evaluation, we follow the Talk2Car C4AV protocol [14] and report IoU for visual grounding; MAE and IoU for spatial reasoning; and Spearman’s (ρ) and Kendall’s (τ) for emotion awareness.

Implementation Details. We train E3AD using the MS-Swift library [79] with LoRA fine-tuning [21] (rank 16, scaling factor 32), a constant learning rate of 10^{-4} , and

Table 1. End-to-end performance of E3AD vs. state-of-the-art (SOTA) baselines. Best results are **bold**; second-best are underlined.

Model	ADE ↓	Fréchet ↓	SSPD ↓	DTW ↓	FDE ↓	PA ₂ ↑	PA ₄ ↑
A*-ROL [20]	5.63 ± 0.12	10.22 ± 0.20	3.06 ± 0.06	93.35 ± 1.80	9.34 ± 0.18	5.45 ± 1.38	25.13 ± 2.63
A*-PE (PDPC) [20]	5.35 ± 0.13	9.38 ± 0.22	2.80 ± 0.07	86.78 ± 2.28	8.22 ± 0.21	25.95 ± 2.66	46.41 ± 3.03
GoalGAN [12]	5.89 ± 0.12	10.86 ± 0.21	3.09 ± 0.06	98.75 ± 2.11	10.08 ± 0.20	17.32 ± 2.30	33.82 ± 2.87
PECNet [77]	4.78 ± 0.10	8.84 ± 0.19	2.54 ± 0.05	76.87 ± 1.75	8.22 ± 0.17	15.59 ± 2.20	37.68 ± 2.94
Y-net [41]	5.28 ± 0.10	10.01 ± 0.19	2.50 ± 0.04	85.25 ± 1.69	8.98 ± 0.18	2.49 ± 0.94	30.84 ± 2.81
TTST [41]	5.24 ± 0.10	9.79 ± 0.19	2.47 ± 0.04	84.02 ± 1.68	8.50 ± 0.18	13.98 ± 2.11	37.54 ± 2.94
CWS [41]	4.82 ± 0.11	9.30 ± 0.20	2.46 ± 0.05	78.69 ± 1.84	8.59 ± 0.18	3.27 ± 1.08	34.66 ± 2.89
TTST + CWS [41]	4.76 ± 0.10	8.95 ± 0.19	2.41 ± 0.05	76.84 ± 1.77	8.08 ± 0.17	17.54 ± 2.31	40.79 ± 2.96
PTPC [18]	<u>4.54 ± 0.11</u>	<u>8.55 ± 0.20</u>	<u>2.18 ± 0.05</u>	<u>72.09 ± 1.86</u>	<u>7.75 ± 0.19</u>	<u>24.46 ± 2.61</u>	<u>45.55 ± 3.03</u>
Qwen2.5-VL-72B [1]	12.51 ± 0.28	26.15 ± 0.52	5.87 ± 0.14	206.99 ± 4.80	25.85 ± 0.55	1.18 ± 0.42	3.13 ± 0.60
Qwen3-VL-8B [69]	14.07 ± 0.30	28.38 ± 0.58	6.65 ± 0.16	234.81 ± 5.20	27.96 ± 0.60	1.89 ± 0.50	4.50 ± 0.70
FSDrive-Finetuned [73]	5.02 ± 0.12	10.98 ± 0.24	2.28 ± 0.06	74.50 ± 2.10	10.45 ± 0.22	17.10 ± 2.40	27.85 ± 2.80
CAVG (+Planner) [34]	4.88 ± 0.14	9.23 ± 0.20	2.20 ± 0.04	73.51 ± 1.42	9.23 ± 0.28	20.10 ± 2.45	43.25 ± 2.63
E3AD (Ours)	3.88 ± 0.10	7.23 ± 0.19	1.86 ± 0.05	60.07 ± 1.69	6.64 ± 0.18	36.21 ± 0.94	55.62 ± 0.95
	17.01% ↑	18.26% ↑	17.20% ↑	16.67% ↑	20.00% ↑	16.71% ↑	18.10% ↑

Table 2. Comparison of E3AD and state-of-the-art baselines on visual grounding tasks. Best results are **bold**; second-best are underlined.

Model	Backbone	Talk2Car	MoCAD		DrivePilot		Corner-case Test sets			Long-text
			test	val	test	val	Visual Constr.	Multi-agent	Ambiguous	val
AttnGrounder [43]	ResNet-50	61.32	62.34	64.35	62.31	64.57	62.74	64.82	64.31	57.25
CMSVG [51]	EfficientNet	68.61	67.66	68.47	68.87	69.93	69.39	66.77	67.83	62.21
TransVG [13]	ResNet-101	65.83	68.14	70.85	66.52	68.42	68.12	66.34	69.25	65.45
CMRT [40]	ResNet-152	69.11	69.42	68.83	69.54	70.37	67.12	66.20	62.23	64.25
MDERT [26]	ResNet-101	70.52	66.74	70.23	71.35	72.15	68.35	65.37	68.38	62.72
VL-BERT [10]	ResNet-101	70.03	71.42	70.54	71.47	72.36	<u>70.29</u>	70.14	69.84	66.70
RSD-LXMERT [4]	ResNet-101	72.64	72.35	71.46	73.37	74.52	70.22	<u>71.87</u>	63.44	65.80
VLTVG [70]	ResNet-101	63.33	67.14	68.26	65.37	68.49	68.51	66.22	70.24	<u>68.80</u>
Grounding-DINO [38]	ViT	68.15	67.92	68.48	69.50	70.10	66.17	65.85	67.24	63.15
UNINEXT [68]	ResNet-50	70.87	70.62	71.34	71.35	73.47	69.26	68.78	<u>71.29</u>	65.32
CAVG [34]	ViT	<u>74.62</u>	<u>72.44</u>	<u>73.25</u>	<u>75.52</u>	<u>76.48</u>	68.39	67.36	69.45	64.36
Qwen2.5-VL-7B [1]	VLM	47.31	48.20	49.10	50.06	50.84	45.12	46.37	47.05	41.92
Qwen2.5-VL-72B [1]	VLM	56.17	57.10	57.85	58.92	59.74	53.43	54.25	55.17	49.83
Qwen3-VL-8B [69]	VLM	56.19	57.25	58.16	59.05	59.85	53.55	54.49	55.25	50.13
E3AD (Ours)	VLM	80.12	80.94	79.64	81.02	82.56	76.62	77.24	77.05	77.86
	–	6.86% ↑	10.50% ↑	8.72% ↑	6.79% ↑	7.36% ↑	8.26% ↑	6.95% ↑	7.48% ↑	11.63% ↑

a per-device batch size of 16 for one epoch over the full dataset. Training is conducted in two stages: (i) modality pretraining and unified fine-tuning to adapt the backbone to domain data, and (ii) behavioral alignment via DPO to refine responses toward the desired driving behavior. All experiments are run on 8×NVIDIA H200 GPUs. To ensure a fair comparison, we freeze the Qwen2.5-VL-7B backbone and train only low-rank adapters, keeping the trainable parameter budget comparable to or smaller than the baselines. The gains in Tables 1–2 thus mainly stem from the proposed emotion modeling, dual-path spatial reasoning, and consistency-oriented training rather than model size. Larger generic VLMs (Qwen2.5-VL-72B, Qwen3-VL-8B) still underperform E3AD, indicating that task-aligned structure and objectives matter more than raw capacity. See Appendix B for more details on experiment setups of the proposed E3AD.

4.2. Joint Evaluation Results

Table 1 reports the end-to-end performance of E3AD and SOTA baselines under unified evaluation settings. In our formulation, emotion perception, spatial understanding, and visual grounding jointly provide intermediate evidence for downstream planning, simulating a more realistic AD pipeline that couples perception, cognition, and action. The results clearly show that E3AD outperforms all baselines across seven standard trajectory metrics. Compared with the strongest baseline (PTPC), our model achieves notable gains of 17.01%, 18.26%, and 20.00% reductions in ADE, Fréchet, and FDE, respectively, indicating more accurate and stable trajectory forecasting. Likewise, E3AD improves SSPD and DTW by over 16%, reflecting better temporal smoothness and spatial coherence in path generation. In planning accuracy, E3AD improves PA₂/PA₄ by +16.71%/+18.10%, indicating tighter

Table 3. Emotion prediction across valence, arousal, and dominance. Reported metrics are Spearman’s ρ and Kendall’s τ correlations with ground-truth VAD (\uparrow : a higher value is better).

Model	Valence \uparrow		Arousal \uparrow		Dominance \uparrow	
	ρ	τ	ρ	τ	ρ	τ
BERT [16] + Ridge	0.78	0.59	0.75	0.56	0.74	0.55
RoBERTa [39] + Ridge	0.80	0.61	0.77	0.59	0.78	0.58
DistilBERT [52] + Ridge	0.82	0.64	0.79	0.61	0.79	0.60
Qwen2.5-7B-Instruct [60]	0.11	0.08	0.02	0.02	0.04	0.03
Qwen3-Emb.-4B [76] + Ridge	0.83	0.64	0.79	0.61	0.82	0.63
E3AD (ours)	0.95	0.84	0.94	0.82	0.94	0.81

Table 4. Spatial reasoning results on Talk2Car vs. VLM baselines.

Model	T2C	Target Loc. Est.			Target Depth Est.		
	IoU ₅₀	MAE \downarrow	PA ₂	PA ₄	MAE \downarrow	PA ₂	PA ₄
Qwen2.5-VL-7B [1]	40.23	3.49	39.5	71.1	22.92	1.3	4.2
Qwen2.5-VL-72B [1]	51.42	10.1	38.5	77.9	22.68	1.5	4.5
Qwen3-VL-8B [69]	52.68	3.71	32.8	71.5	18.89	13.7	26.5
E3AD (Ours)	79.32	0.47	97.7	98.8	4.25	53.1	71.2

alignment between plans and driving goals. General-purpose VLMs (Qwen-VL) still struggle, and FSDrive-Finetuned trails markedly, with higher FDE (10.45 vs. 6.64), confirming the limitations of existing VLA models in handling command-driven scenarios. Overall, E3AD’s stronger fusion of command semantics, spatial context, and emotion yields more reliable and command-aligned waypoint planning.

4.3. Sub-task Evaluation Results

We report the performance of E3AD on key sub-tasks against SOTA methods. Notably, our model addresses all tasks concurrently within one end-to-end trained network, whereas other baselines are specialized for only one task.

Visual Grounding. Table 2 reports visual grounding results. E3AD surpasses the strongest baseline (CAVG) with absolute gains of +6.86% (Talk2Car), +10.50% / +8.72% (MoCAD test/val), and +6.79% / +7.36% (DrivePilot test/val). This superiority is especially pronounced in challenging scenes. On corner-case splits (occluded, multi-agent, ambiguous), it improves by +8.26%, +6.95%, and +7.48%, and on Long-text by +11.63%. Generic VLMs (Qwen) lag markedly across all datasets. These results indicate that our emotion- and spatial-aware grounding yields more precise and robust localization within a unified end-to-end model.

Spatial Reasoning. Table 4 illustrates that E3AD markedly outperforms large VLM baselines (Qwen2.5/3-VL) on target localization and depth estimation. While even VLMs like Qwen2.5-VL-72B struggle with basic spatial reasoning (Location MAE 10.1, Depth MAE 22.68), E3AD demonstrates a precise, grounded understanding with an MAE of only 0.47 (Location) and 4.25 (Depth), respectively. This superiority is consistent in accuracy metrics, where E3AD achieves 97.7% PA₂ (Location) and 53.1% PA₂ (Depth), far above the best VLM. These results demonstrate that E3AD establishes a

Table 5. Ablation study of E3AD’s core components on visual grounding performance on the Talk2Car (T2C) benchmark, vision constraint (Constr.), ambiguous (Ambg.), and long-context command (Long) test sets. Components: Egocentric pathway (Ego.), Allocentric pathway (Allo.), DPO, and Emotion Modeling (Emo.).

Ego.	Allo.	Emo.	DPO	T2C \uparrow	Constr. \uparrow	Ambg. \uparrow	Long \uparrow
\times	\checkmark	\checkmark	\checkmark	74.48	71.60	72.24	72.47
\checkmark	\times	\checkmark	\checkmark	76.48	73.92	74.65	74.76
\checkmark	\checkmark	\times	\checkmark	78.78	74.41	73.57	74.12
\checkmark	\checkmark	\checkmark	\times	79.55	75.58	77.09	76.44
\checkmark	\checkmark	\checkmark	\checkmark	80.12	76.62	77.05	77.86

Table 6. Ablation of core designs in E3AD on waypoint planning.

Ego.	Allo.	Emo.	DPO	ADE \downarrow	SSPD \downarrow	Fréchet \downarrow	FDE \downarrow
\times	\checkmark	\checkmark	\checkmark	4.12	2.06	7.61	7.02
\checkmark	\times	\checkmark	\checkmark	4.27	2.15	7.86	7.31
\checkmark	\checkmark	\times	\checkmark	3.93	1.91	7.36	6.80
\checkmark	\checkmark	\checkmark	\times	3.96	1.89	7.31	6.86
\checkmark	\checkmark	\checkmark	\checkmark	3.88	1.86	7.23	6.64

new state of the art in fine-grained 3D spatial perception and localization, significantly outperforming conventional visual-spatial VLMs in real-world driving scenarios.

Emotion Recognition. Table 3 presents emotion recognition results across valence, arousal, and dominance dimensions. Since VAD represents relative rather than absolute emotional magnitudes, we adopt Spearman’s rank correlation (ρ) and Kendall’s rank correlation coefficient (τ) as evaluation metrics to assess the monotonic relationship between model predictions and labels. The *Ridge* regressor obtains command embeddings from language models and applies ridge regression to predict continuous VAD values, serving as a lightweight emotion estimator. E3AD achieves the highest correlation with human annotations, reaching 0.95/0.84 (ρ , τ) for valence, 0.94/0.82 for arousal, and 0.94/0.81 for dominance. In contrast, Qwen2.5-7B and Qwen3-4B exhibit near-random correlation levels, revealing limited sensitivity to emotion cues. These results show that E3AD effectively models the continuous emotion space of human emotions, capturing valence (positive-negative sentiment), arousal (intensity), and dominance (sense of control), enabling human-centric planning and verbal feedback for passengers.

4.4. Ablation Study

Table 5 summarizes module contributions. Removing the egocentric pathway causes the largest VG drop ($\downarrow 7.0\%$ IoU on Talk2Car; $\downarrow 6.6\%$ on Vision-Constraint), confirming its role in first-person grounding that aligns linguistic references with observed targets. Excluding the allocentric map weakens global reasoning by removing complementary spatial semantics and scene topology. The Emotion Modeling branch shows the greatest benefit on ambiguous and long-text commands (+4.5% and +4.8%), enhancing the model’s sensitivity to nuanced linguistic cues and emotionally rich ex-

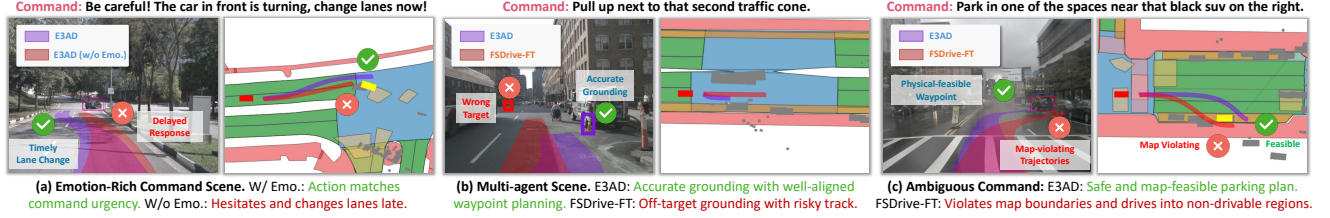


Figure 4. Qualitative comparison between E3AD and FSDrive-FT in emotion-rich (a), multi-agent (b), and ambiguous (c) scenes.

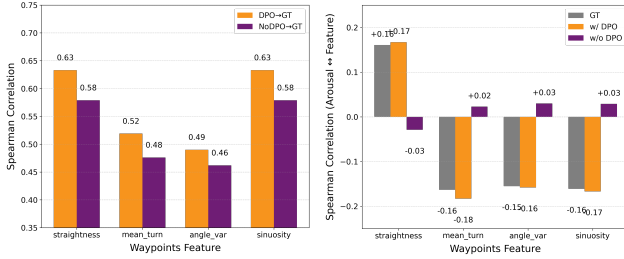


Figure 5. DPO's effect on emotion-trajectory consistency.

pressions. DPO gives moderate gains by refining multimodal alignment. For waypoint planning (Table 6), the allocentric map is critical: removal degrades trajectories (ADE/FDE ($\uparrow 10.0\%/\uparrow 10.1\%$)), indicating the value of global priors for spatial awareness and route consistency. The egocentric path-way anchors local motion cues; Emotion Modeling and DPO further improve robustness and smoothness.

As in Fig. 5, DPO raises Spearman correlations for straightness/sinuosity and stabilizes turn smoothness and angular variation, yielding geometrically coherent, behaviorally consistent paths. Higher arousal corresponds to straighter, smoother motion; lower arousal to more cautious, curved motion. Overall, DPO strengthens emotion-trajectory consistency even when numeric gains are modest.

4.5. Case Study

Fig. 6 illustrates how E3AD integrates emotion understanding with spatial reasoning to produce end-to-end behavior. The VAD plot showcases that the Emotion Modeling component captures the linguistic shift from a neutral command to its cautious variant: the neutral command maps to (0.60, 0.39, 0.45), while adding the qualifier “Be more cautious” shifts the VAD state to (0.60, 0.49, 0.51), increasing Arousal and Dominance. Conditioned on the neutral VAD, E3AD plans a standard lane-change maneuver; conditioned on the cautious VAD, the DPO-aligned policy instead avoids the lane change altogether. The generated textual feedback is also conditioned on emotion state \hat{e} : the EmoThink block infers a cautious, slightly anxious passenger and produces a reassuring explanation rather than a neutral one.

Taken together with the geometric statistics in Fig. 5, these results indicate that emotion supervision affects not only language but also motion geometry. At fixed intent, higher arousal steers E3AD toward straighter paths with

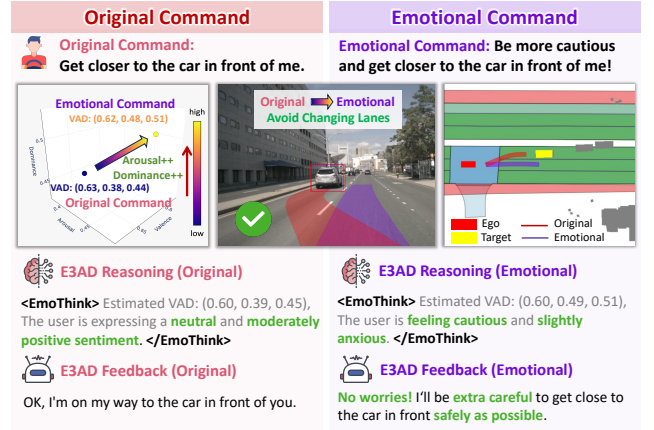


Figure 6. Case study for the impact of different emotional commands (neutral vs. cautious) on E3AD's end-to-end performance.

less lateral oscillation and earlier hazard avoidance, while lower arousal produces slower approaches with larger safety margins. Thus, the VAD vector acts as a continuous control signal selecting among behaviorally distinct yet physically valid plans, rather than as a binary switch or style token.

4.6. Qualitative Analysis

Fig. 4 showcases qualitative comparisons between E3AD and FSDrive-FT [73] across three challenging scenes. In the emotion-rich command scene (Panel (a)), E3AD leverages its continuous VAD-based emotion modeling to infer the passenger's heightened urgency and produces a timely lane-change response. In contrast, the variant without emotion modeling hesitates, reacting too late. In the multi-agent scene (Panel (b)), where objects are partially occluded and visual cues are ambiguous, E3AD integrates allocentric topology with ego-centric evidence via its spatial reasoning, enabling correct target grounding and a safe, well-aligned trajectory. FSDrive-FT fails to parse the complex scene structure, resulting in off-target grounding and unsafe plans. In the ambiguous command scene (panel (c)), E3AD resolves linguistic ambiguity by combining language tone with spatial context, producing a feasible, map-consistent parking path, whereas FSDrive-FT crosses map boundaries into non-drivable regions. Overall, this illustrates how emotion-aware language understanding and dual-frame spatial reasoning enable E3AD to deliver more interpretable and human-aligned grounding and plan-

ning. See Appendix D for more qualitative results of E3AD.

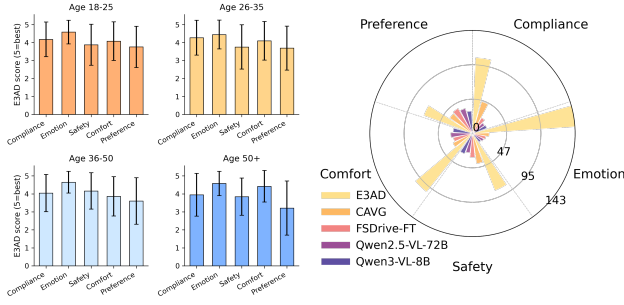


Figure 7. User study on perceived compliance, emotion, safety, and preference. (Left) E3AD consistently achieves high Likert scores across all age groups. (Right) Comparison of Rank-1 votes, E3AD dominates in most dimensions, outperforming all baselines.

4.7. User Study

To evaluate the real-world utility of E3AD, we conduct a user study with 217 participants (details are available in Appendix C). Participants viewed anonymized clips from five systems and ranked them on Command Compliance, Emotion Alignment, Safety, Comfort, and Overall Preference. As shown in Fig. 7, E3AD obtains the highest mean scores and most Rank-1 votes on most dimensions, indicating a clear preference over the baselines. Beyond absolute scores, participants consistently prefer trajectories that match the command’s emotional tone, maintain correct grounding, and stay physically feasible. Systems without emotion modeling (FSDrive-FT, generic VLMs) are often seen as hesitant or unsafe, whereas E3AD’s emotion-aware grounding and map-feasible planning are judged more confident and trustworthy, highlighting the value of emotion cues in end-to-end AD.

5. Conclusion and Future Work

This work extends end-to-end AD from purely rational control to emotion-aware grounding and planning. We introduce Open-Domain End-to-End AD and propose E3AD, a VLA framework that couples continuous VAD-based emotion modeling, dual-pathway spatial reasoning, and consistency-oriented training. Experiments on four real-world benchmarks show consistent improvements in visual grounding, trajectory quality, and continuous emotion estimation over strong baselines. In future work, we plan to incorporate real human preference feedback, richer multimodal emotion signals beyond language, and closed-loop evaluation in high-fidelity simulators to further enhance the reliability and acceptance of emotion-aware autonomous driving systems.

References

- [1] Shuai Bai, Keqin Chen, Xuejing Liu, Jialin Wang, Wenbin Ge, Sibao Song, Kai Dang, Peng Wang, Shijie Wang, Jun Tang, et al. Qwen2. 5-vl technical report. *arXiv preprint arXiv:2502.13923*, 2025. 3, 6, 7
- [2] Neil Burgess. Spatial memory: how egocentric and allocentric combine. *Trends in cognitive sciences*, 10(12):551–557, 2006. 4
- [3] Holger Caesar, Varun Bankiti, Alex H Lang, Sourabh Vora, Venice Erin Liong, Qiang Xu, Anush Krishnan, Yu Pan, Giancarlo Baldan, and Oscar Beijbom. nuscenes: A multi-modal dataset for autonomous driving. In *Proceedings of the IEEE/CVF CVPR*, pages 11621–11631, 2020. 14
- [4] Hou Pong Chan, Mingxi Guo, and Cheng-Zhong Xu. Grounding commands for autonomous vehicles via layer fusion with region-specific dynamic layer attention. In *2022 IEEE/RSJ International Conference on Intelligent Robots and Systems (IROS)*, pages 12464–12470. IEEE, 2022. 6
- [5] Jielin Chen, Xuefen Lin, Weifeng Ma, Yuchen Wang, and Wei Tang. Eeg-based emotion recognition for road accidents in a simulated driving environment. *Biomedical signal processing and control*, 87:105411, 2024. 2
- [6] Li Chen, Penghao Wu, Kashyap Chitta, Bernhard Jaeger, Andreas Geiger, and Hongyang Li. End-to-end autonomous driving: Challenges and frontiers. *IEEE Transactions on Pattern Analysis and Machine Intelligence*, 2024. 1
- [7] Xingtong Chen, Xia Wang, Cong Fang, Le Fang, Wei Gong, Chengzhong Liu, and Stephen Jia Wang. Emotion-aware design in automobiles: Embracing technology advancements to enhance human-vehicle interaction. In *Proceedings of the 2025 CHI Conference on Human Factors in Computing Systems*, pages 1–18, 2025. 1
- [8] Roddy Cowie, Ellen Douglas-Cowie, Nicolas Tsapatsoulis, George Votsis, Stefanos Kollias, Winfried Fellenz, and John G Taylor. Emotion recognition in human-computer interaction. *IEEE Signal processing magazine*, 18(1):32–80, 2001. 2
- [9] Can Cui, Yunsheng Ma, Xu Cao, Wenqian Ye, Yang Zhou, Kaizhao Liang, Jintai Chen, Juanwu Lu, Zichong Yang, Kuei-Da Liao, et al. A survey on multimodal large language models for autonomous driving. In *Proceedings of the IEEE/CVF winter conference on applications of computer vision*, pages 958–979, 2024. 2
- [10] Hang Dai, Shujie Luo, Yong Ding, and Ling Shao. Commands for autonomous vehicles by progressively stacking visual-linguistic representations. In *Computer Vision–ECCV Workshops*, pages 27–32, 2020. 6
- [11] Dorottya Demszky, Dana Movshovitz-Attias, Jeongwoo Ko, Alan Cowen, Gaurav Nemade, and Sujith Ravi. Goemotions: A dataset of fine-grained emotions. *arXiv preprint arXiv:2005.00547*, 2020. 4
- [12] Patrick Dendorfer, Aljosa Osep, and Laura Leal-Taixé. Goalgan: Multimodal trajectory prediction based on goal position estimation. In *Proceedings of the Asian Conference on Computer Vision*, 2020. 6
- [13] Jiajun Deng, Zhengyuan Yang, Tianlang Chen, Wengang Zhou, and Houqiang Li. Transvg: End-to-end visual ground-

- ing with transformers. In *Proceedings of the IEEE/CVF ICCV*, pages 1769–1779, 2021. 6
- [14] Thierry Deruyttere, Simon Vandenhende, Dusan Grujicic, Luc Van Gool, and Marie-Francine Moens. Talk2car: Taking control of your self-driving car. *arXiv preprint arXiv:1909.10838*, 2019. 5, 14
- [15] Thierry Deruyttere, Dusan Grujicic, Matthew B Blaschko, and Marie-Francine Moens. Talk2car: Predicting physical trajectories for natural language commands. *Ieee Access*, 10: 123809–123834, 2022. 5, 14, 15
- [16] Jacob Devlin, Ming-Wei Chang, Kenton Lee, and Kristina Toutanova. Bert: Pre-training of deep bidirectional transformers for language understanding. In *Proceedings of the 2019 conference of the North American chapter of the association for computational linguistics: human language technologies, volume 1 (long and short papers)*, pages 4171–4186, 2019. 7
- [17] Marvin Gaertner, Daniel Sauter, Hermann Baumgartl, Thilo Rieg, and Ricardo Buettner. Multi-class emotion recognition within the valence-arousal-dominance space using eeg. In *AMCIS*, 2021. 2
- [18] Dusan Grujicic, Thierry Deruyttere, Marie-Francine Moens, and Matthew B Blaschko. Predicting physical world destinations for commands given to self-driving cars. In *Proceedings of the AAAI Conference on Artificial Intelligence*, pages 715–725, 2022. 5, 6
- [19] Liao Haicheng, Shen Huanming, Wang Bonan, Li Yongkang, Tang Yihong, Wang Chengyue, Zhuang Dingyi, Chen Kehua, Yang Hai, Xu Chengzhong, and Li Zhenning. Think before you drive: World model-inspired multimodal grounding for autonomous driving. *arXiv preprint*, 2025. 5, 14
- [20] Peter E Hart, Nils J Nilsson, and Bertram Raphael. A formal basis for the heuristic determination of minimum cost paths. *IEEE transactions on Systems Science and Cybernetics*, 4(2): 100–107, 1968. 6
- [21] Edward J. Hu, Yelong Shen, Phillip Wallis, Zeyuan Allen-Zhu, Yuanzhi Li, Shean Wang, Lu Wang, and Weizhu Chen. Lora: Low-rank adaptation of large language models. In *ICLR*, 2022. 5
- [22] Yihan Hu, Jiazhi Yang, Li Chen, Keyu Li, Chonghao Sima, Xizhou Zhu, Siqi Chai, Senyao Du, Tianwei Lin, Wenhai Wang, et al. Planning-oriented autonomous driving. In *Proceedings of the IEEE/CVF Conference on Computer Vision and Pattern Recognition*, pages 17853–17862, 2023. 1
- [23] Xiaosong Jia, Penghao Wu, Li Chen, Jiangwei Xie, Conghui He, Junchi Yan, and Hongyang Li. Think twice before driving: Towards scalable decoders for end-to-end autonomous driving. In *Proceedings of the IEEE/CVF Conference on Computer Vision and Pattern Recognition*, pages 21983–21994, 2023. 1
- [24] Bo Jiang, Shaoyu Chen, Bencheng Liao, Xingyu Zhang, Wei Yin, Qian Zhang, Chang Huang, Wenyu Liu, and Xinggang Wang. Senna: Bridging large vision-language models and end-to-end autonomous driving. *arXiv preprint arXiv:2410.22313*, 2024. 2
- [25] Sicong Jiang, Zilin Huang, Kangan Qian, Ziang Luo, Tianze Zhu, Yang Zhong, Yihong Tang, Menglin Kong, Yunlong Wang, Siwen Jiao, et al. A survey on vision-language-action models for autonomous driving. *arXiv preprint arXiv:2506.24044*, 2025. 1, 2
- [26] Aishwarya Kamath, Mannat Singh, Yann LeCun, Gabriel Synnaeve, Ishan Misra, and Nicolas Carion. Mdetr-modulated detection for end-to-end multi-modal understanding. In *Proceedings of the IEEE/CVF ICCV*, pages 1780–1790, 2021. 6
- [27] Seungji Lee, Taejun Lee, Taeyang Yang, Changrak Yoon, and Sung-Phil Kim. Detection of drivers’ anxiety invoked by driving situations using multimodal biosignals. *Processes*, 8 (2):155, 2020. 3
- [28] Wenbo Li, Guofa Li, Ruichen Tan, Cong Wang, Zemin Sun, Ying Li, Gang Guo, Dongpu Cao, and Keqiang Li. Review and perspectives on human emotion for connected automated vehicles. *Automotive Innovation*, 7(1):4–44, 2024. 2
- [29] Yingyan Li, Shuyao Shang, Weisong Liu, Bing Zhan, Haochen Wang, Yuqi Wang, Yuntao Chen, Xiaoman Wang, Yasong An, Chufeng Tang, et al. Drivevla-w0: World models amplify data scaling law in autonomous driving. *arXiv preprint arXiv:2510.12796*, 2025. 1
- [30] Yue Li, Meng Tian, Zhenyu Lin, Jiangtong Zhu, Dechang Zhu, Haiqiang Liu, Yueyi Zhang, Zhiwei Xiong, and Xinhai Zhao. Fine-grained evaluation of large vision-language models in autonomous driving. In *Proceedings of the IEEE/CVF International Conference on Computer Vision*, pages 9431–9442, 2025. 2
- [31] Yongkang Li, Kaixin Xiong, Xiangyu Guo, Fang Li, Sixu Yan, Gangwei Xu, Lijun Zhou, Long Chen, Haiyang Sun, Bing Wang, et al. Recogdrive: A reinforced cognitive framework for end-to-end autonomous driving. *arXiv preprint arXiv:2506.08052*, 2025. 1
- [32] Zhenning Li, Zhiyong Cui, Haicheng Liao, John Ash, Guohui Zhang, Chengzhong Xu, and Yinhai Wang. Steering the future: Redefining intelligent transportation systems with foundation models. *Chain*, 1(1):46–53, 2024. 1, 2
- [33] Yuheng Liang, Zheyu Wang, Feng Liu, Mingzhou Liu, and Yu Yao. Mamba-va: A mamba-based approach for continuous emotion recognition in valence-arousal space. In *Proceedings of the Computer Vision and Pattern Recognition Conference*, pages 5651–5656, 2025. 3
- [34] Haicheng Liao, Huanming Shen, Zhenning Li, Chengyue Wang, Guofa Li, Yiming Bie, and Chengzhong Xu. Gpt-4 enhanced multimodal grounding for autonomous driving: Leveraging cross-modal attention with large language models. *Communications in Transportation Research*, 4:100116, 2024. 3, 5, 6, 14
- [35] Haicheng Liao, Hanlin Kong, Bonan Wang, Chengyue Wang, Wang Ye, Zhengbing He, Chengzhong Xu, and Zhenning Li. Cot-drive: Efficient motion forecasting for autonomous driving with llms and chain-of-thought prompting. *IEEE Transactions on Artificial Intelligence*, 2025. 2
- [36] Haicheng Liao, Zhenning Li, Guohui Zhang, Keqiang Li, and Chengzhong Xu. Toward human-like trajectory prediction for autonomous driving: A behavior-centric approach. *Transportation Science*, 2025. 1
- [37] Pei Liu, Qingtian Ning, Xinyan Lu, Haipeng Liu, Weiliang Ma, Dangen She, Peng Jia, Xianpeng Lang, and Jun Ma. Omnireason: A temporal-guided vision-language-action framework for autonomous driving. *arXiv preprint arXiv:2509.00789*, 2025. 2

- [38] Shilong Liu, Zhaoyang Zeng, Tianhe Ren, Feng Li, Hao Zhang, Jie Yang, Chunyuan Li, Jianwei Yang, Hang Su, Jun Zhu, et al. Grounding dino: Marrying dino with grounded pre-training for open-set object detection. *arXiv preprint arXiv:2303.05499*, 2023. 6
- [39] Yinhan Liu, Myle Ott, Naman Goyal, Jingfei Du, Mandar Joshi, Danqi Chen, Omer Levy, Mike Lewis, Luke Zettlemoyer, and Veselin Stoyanov. Roberta: A robustly optimized bert pretraining approach. *arXiv preprint arXiv:1907.11692*, 2019. 7
- [40] Shujie Luo, Hang Dai, Ling Shao, and Yong Ding. C4av: learning cross-modal representations from transformers. In *Computer Vision–ECCV 2020*, pages 33–38, 2020. 6
- [41] Karttikeya Mangalam, Yang An, Harshayu Girase, and Jitendra Malik. From goals, waypoints & paths to long term human trajectory forecasting. In *Proceedings of the IEEE/CVF international conference on computer vision*, pages 15233–15242, 2021. 6
- [42] Gerald Matthews, Lisa Dorn, and A Ian Glendon. Personality correlates of driver stress. *Personality and Individual Differences*, 12(6):535–549, 1991. 4
- [43] Vivek Mittal. Attngrounder: Talking to cars with attention. In *Computer Vision–ECCV Workshops*, pages 62–73, 2020. 6
- [44] Saif M. Mohammad. Obtaining reliable human ratings of valence, arousal, and dominance for 20,000 english words. In *Proceedings of The Annual Conference of the Association for Computational Linguistics (ACL)*, Melbourne, Australia, 2018. 13
- [45] Luntian Mou, Yiyuan Zhao, Chao Zhou, Bahareh Nakisa, Mohammad Naim Rastgoo, Lei Ma, Tiejun Huang, Baocai Yin, Ramesh Jain, and Wen Gao. Driver emotion recognition with a hybrid attentional multimodal fusion framework. *IEEE Transactions on Affective Computing*, 14(4):2970–2981, 2023. 2
- [46] Tong Nie, Yuewen Mei, Yihong Tang, Junlin He, Jie Sun, Haotian Shi, Wei Ma, and Jian Sun. Steerable adversarial scenario generation through test-time preference alignment. *arXiv preprint arXiv:2509.20102*, 2025. 1
- [47] Chenbin Pan, Burhaneddin Yaman, Tommaso Nesti, Abhirup Mallik, Alessandro G Allievi, Senem Velipasalar, and Liu Ren. Vlp: Vision language planning for autonomous driving. In *Proceedings of the IEEE/CVF Conference on Computer Vision and Pattern Recognition*, pages 14760–14769, 2024. 2
- [48] Aditya Prakash, Kashyap Chitta, and Andreas Geiger. Multi-modal fusion transformer for end-to-end autonomous driving. In *Proceedings of the IEEE/CVF conference on computer vision and pattern recognition*, pages 7077–7087, 2021. 1
- [49] Rafael Rafailov, Archit Sharma, Eric Mitchell, Christopher D Manning, Stefano Ermon, and Chelsea Finn. Direct preference optimization: Your language model is secretly a reward model. *Advances in neural information processing systems*, 36:53728–53741, 2023. 5
- [50] Katrin Renz, Long Chen, Elahe Arani, and Oleg Sinavski. Simlingo: Vision-only closed-loop autonomous driving with language-action alignment. In *Proceedings of the Computer Vision and Pattern Recognition Conference*, pages 11993–12003, 2025. 2
- [51] Nivedita Rufus, Unni Krishnan R Nair, K Madhava Krishna, and Vineet Gandhi. Cosine meets softmax: A tough-to-beat baseline for visual grounding. In *Computer Vision–ECCV Workshops*, pages 39–50, 2020. 6
- [52] Victor Sanh, Lysandre Debut, Julien Chaumond, and Thomas Wolf. Distilbert, a distilled version of bert: smaller, faster, cheaper and lighter. *arXiv preprint arXiv:1910.01108*, 2019. 7
- [53] Ranjan Sapkota, Yang Cao, Konstantinos I Roumeliotis, and Manoj Karkee. Vision-language-action models: Concepts, progress, applications and challenges. *arXiv preprint arXiv:2505.04769*, 2025. 2
- [54] Hao Shao, Yuxuan Hu, Letian Wang, Guanglu Song, Steven L Waslander, Yu Liu, and Hongsheng Li. Lmdrive: Closed-loop end-to-end driving with large language models. In *Proceedings of the IEEE/CVF Conference on Computer Vision and Pattern Recognition*, pages 15120–15130, 2024. 2
- [55] Jacopo Sini, Antonio Costantino Marceddu, Massimo Violante, and Riccardo Dessì. Passengers’ emotions recognition to improve social acceptance of autonomous driving vehicles. In *Progresses in Artificial Intelligence and Neural Systems*, pages 25–32. Springer, 2020. 2
- [56] Liang Tan, Keping Yu, Long Lin, Xiaofan Cheng, Gautam Srivastava, Jerry Chun-Wei Lin, and Wei Wei. Speech emotion recognition enhanced traffic efficiency solution for autonomous vehicles in a 5g-enabled space–air–ground integrated intelligent transportation system. *IEEE Transactions on Intelligent Transportation Systems*, 23(3):2830–2842, 2021. 2
- [57] Yihong Tang and Wei Ma. Intent: Trajectory prediction framework with intention-guided contrastive clustering. *arXiv preprint arXiv:2503.04952*, 2025. 2
- [58] Yihong Tang, Zhaokai Wang, Ao Qu, Yihao Yan, Zhaofeng Wu, Dingyi Zhuang, Jushi Kai, Kebing Hou, Xiaotong Guo, Jinhua Zhao, et al. Itinera: Integrating spatial optimization with large language models for open-domain urban itinerary planning. In *Proceedings of the 2024 Conference on Empirical Methods in Natural Language Processing: Industry Track*, pages 1413–1432, 2024. 2
- [59] Yihong Tang, Ao Qu, Zhaokai Wang, Dingyi Zhuang, Zhaofeng Wu, Wei Ma, Shenhao Wang, Yunhan Zheng, Zhan Zhao, and Jinhua Zhao. Sparkle: Mastering basic spatial capabilities in vision language models elicits generalization to spatial reasoning. In *Findings of the Association for Computational Linguistics: EMNLP 2025*, pages 4083–4103, 2025. 2
- [60] Qwen Team. Qwen2.5: A party of foundation models, 2024. 7
- [61] Xiaoyu Tian, Junru Gu, Bailin Li, Yicheng Liu, Yang Wang, Zhiyong Zhao, Kun Zhan, Peng Jia, Xianpeng Lang, and Hang Zhao. Drivevlm: The convergence of autonomous driving and large vision-language models. *arXiv preprint arXiv:2402.12289*, 2024. 1
- [62] Tai Wang, Xinge Zhu, Jiangmiao Pang, and Dahua Lin. Fcos3d: Fully convolutional one-stage monocular 3d object detection. In *Proceedings of the IEEE/CVF international conference on computer vision*, pages 913–922, 2021. 14

- [63] Amy Beth Warriner, Victor Kuperman, and Marc Brysbaert. Norms of valence, arousal, and dominance for 13,915 english lemmas. *Behavior research methods*, 45(4):1191–1207, 2013. 4
- [64] Guoliang Xiang, Song Yao, Xianhui Wu, Hanwen Deng, Guojie Wang, Yu Liu, Fan Li, and Yong Peng. Driver multi-task emotion recognition network based on multi-modal facial video analysis. *Pattern Recognition*, 161:111241, 2025. 3
- [65] Huafei Xiao, Wenbo Li, Guanzhong Zeng, Yingzhang Wu, Jiyong Xue, Juncheng Zhang, Chengmou Li, and Gang Guo. On-road driver emotion recognition using facial expression. *Applied Sciences*, 12(2):807, 2022. 2
- [66] Shuo Xing, Chengyuan Qian, Yuping Wang, Hongyuan Hua, Kexin Tian, Yang Zhou, and Zhengzhong Tu. Openemmas: Open-source multimodal model for end-to-end autonomous driving. In *Proceedings of the Winter Conference on Applications of Computer Vision*, pages 1001–1009, 2025. 2
- [67] Zhenhua Xu, Yujia Zhang, Enze Xie, Zhen Zhao, Yong Guo, Kwan-Yee K Wong, Zhenguo Li, and Hengshuang Zhao. Drivegpt4: Interpretable end-to-end autonomous driving via large language model. *IEEE Robotics and Automation Letters*, 2024. 2
- [68] Bin Yan, Yi Jiang, Jiannan Wu, Dong Wang, Ping Luo, Zehuan Yuan, and Huchuan Lu. Universal instance perception as object discovery and retrieval. In *Proceedings of the IEEE/CVF CVPR*, pages 15325–15336, 2023. 6
- [69] An Yang, Anfeng Li, Baosong Yang, Beichen Zhang, Binyuan Hui, Bo Zheng, Bowen Yu, Chang Gao, Chengen Huang, Chenxu Lv, et al. Qwen3 technical report. *arXiv preprint arXiv:2505.09388*, 2025. 6, 7
- [70] Li Yang, Yan Xu, Chunfeng Yuan, Wei Liu, Bing Li, and Weiming Hu. Improving visual grounding with visual-linguistic verification and iterative reasoning. In *Proceedings of the IEEE/CVF CVPR*, pages 9499–9508, 2022. 6
- [71] Yi Yang, Qingwen Zhang, Ci Li, Daniel Simões Marta, Nazre Batool, and John Folkesson. Human-centric autonomous systems with llms for user command reasoning. In *Proceedings of the IEEE/CVF Winter Conference on Applications of Computer Vision*, pages 988–994, 2024. 3
- [72] Zhenjie Yang, Yilin Chai, Xiaosong Jia, Qifeng Li, Yuqian Shao, Xuekai Zhu, Haisheng Su, and Junchi Yan. Drivemoe: Mixture-of-experts for vision-language-action model in end-to-end autonomous driving. *arXiv preprint arXiv:2505.16278*, 2025. 1
- [73] Shuang Zeng, Xinyuan Chang, Mengwei Xie, Xinran Liu, Yifan Bai, Zheng Pan, Mu Xu, and Xing Wei. Futuresightdrive: Thinking visually with spatio-temporal cot for autonomous driving. *arXiv preprint arXiv:2505.17685*, 2025. 2, 6, 8
- [74] Sebastian Zepf, Javier Hernandez, Alexander Schmitt, Wolfgang Minker, and Rosalind W Picard. Driver emotion recognition for intelligent vehicles: A survey. *ACM Computing Surveys (CSUR)*, 53(3):1–30, 2020. 1
- [75] Jieshu Zhang, Raja Ariffin Bin Raja Ghazilla, Hwa Jen Yap, and Woun Yoong Gan. A comprehensive review: Multisensory and cross-cultural approaches to driver emotion modulation in vehicle systems. *Applied Sciences*, 14(15):6819, 2024. 1
- [76] Yanzhao Zhang, Mingxin Li, Dingkun Long, Xin Zhang, Huan Lin, Baosong Yang, Pengjun Xie, An Yang, Dayiheng Liu, Junyang Lin, et al. Qwen3 embedding: Advancing text embedding and reranking through foundation models. *arXiv preprint arXiv:2506.05176*, 2025. 7
- [77] He Zhao and Richard P Wildes. Where are you heading? dynamic trajectory prediction with expert goal examples. In *Proceedings of the IEEE/CVF International Conference on Computer Vision*, pages 7629–7638, 2021. 6
- [78] Jingyuan Zhao, Yuyan Wu, Rui Deng, Susu Xu, Jinpeng Gao, and Andrew Burke. A survey of autonomous driving from a deep learning perspective. *ACM Computing Surveys*, 57(10):1–60, 2025. 1
- [79] Yuze Zhao, Jintao Huang, Jinghan Hu, Daoze Zhang, Zeyinzi Jiang, Zhikai Wu, Baole Ai, Ang Wang, Wenmeng Zhou, and Yingda Chen. Swift: A scalable lightweight infrastructure for fine-tuning. *arXiv preprint arXiv:2408.05517*, 2024. 5
- [80] Xingcheng Zhou, Xuyuan Han, Feng Yang, Yunpu Ma, and Alois C Knoll. Opendrivevla: Towards end-to-end autonomous driving with large vision language action model. *arXiv preprint arXiv:2503.23463*, 2025. 2
- [81] Zewei Zhou, Tianhui Cai, Seth Z Zhao, Yun Zhang, Zhiyu Huang, Bolei Zhou, and Jiaqi Ma. Autovla: A vision-language-action model for end-to-end autonomous driving with adaptive reasoning and reinforcement fine-tuning. *Nips*, 2025. 2

Appendix

A. Data Construction

A.1. VAD Label Construction

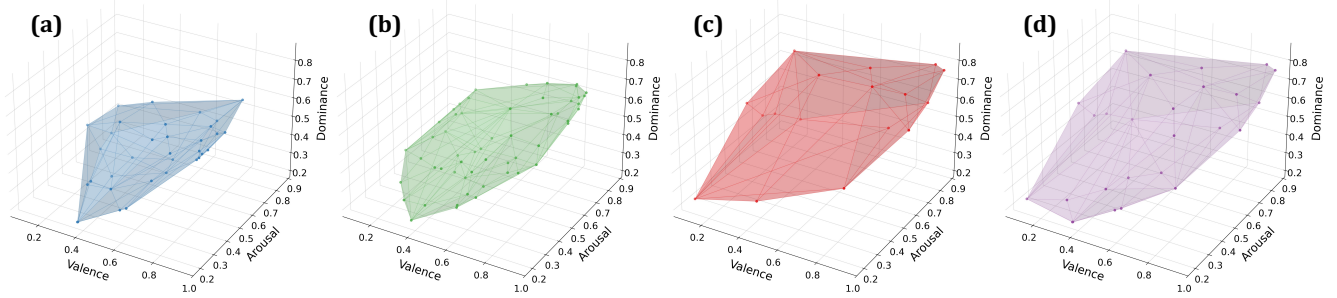


Figure A1. Visualization of the VAD space coverage using 3D convex hulls. (a) The hull of the Original commands (Blue) is concentrated in the neutral region, showing limited emotional diversity. (b) The Augmented commands (Green) significantly expand the volume, introducing more varied emotional states. (c) The hull of the discrete GoEmotions labels (Red) outlines the semantic boundaries of standard emotion categories. (d) The final Union (Purple) of our dataset covers a comprehensive volume of the affective space, ensuring the model is trained on a continuous spectrum of Valence, Arousal, and Dominance.

To capture the subtle emotional nuances in natural language commands, we construct continuous Valence-Arousal-Dominance (VAD) labels using a hybrid fusion strategy that combines sentence-level sentiment analysis with word-level lexical grounding. As implemented in our data processing pipeline, the final VAD vector e is computed as a weighted average of two sources:

Sentence-Level Inference (GoEmotions) We utilize a RoBERTa-based classifier fine-tuned on the GoEmotions dataset (SamLowe/roberta-base-go_emotions)¹ to predict probability scores for 28 discrete emotion categories (e.g., joy, anxiety, neutrality). We map these discrete labels to the continuous VAD space using the NRC-VAD Lexicon [44]. For a given command, the sentence-level VAD vector e_{goe} is calculated as the weighted average of the VAD values of the predicted labels, weighted by their confidence scores.

Word-Level Inference (TF-IDF + Heuristics) To capture keyword-specific emotional intensity, we tokenize the command and filter stop words. We compute a word-level VAD vector e_{words} by averaging the NRC-VAD² values of the remaining tokens, weighted by their TF-IDF scores calculated over the entire corpus. Additionally, we apply a heuristic “Exclamation Boost” to the Arousal dimension. If the command contains exclamation marks, the Arousal score is incrementally increased to reflect heightened urgency.

Fusion and Coverage The final label is obtained via linear fusion: $e_{\text{final}} = \alpha \times e_{\text{goe}} + (1 - \alpha) \times e_{\text{words}}$, with $\alpha = 0.5$. To validate the effectiveness of our emotion-aware data augmentation, we visualize the convex hulls of the resulting VAD vectors in Figure A1. As shown in (a), the original Talk2Car commands (Blue) occupy a narrow, mostly neutral region of the affective space. (b) Our augmentation strategy (Green) significantly expands this coverage. (c) The GoEmotions prior (Red) represents the theoretical space spanned by discrete emotion categories. (d) The final union of data (Purple) demonstrates that our approach successfully covers a broad, continuous spectrum of the VAD space, enabling the model to learn diverse emotional representations.

A.2. Spatial Reasoning Data Construction

To support the multi-task instruction tuning of E3AD, we processed the raw annotations from the Talk2Car-Trajectory dataset into standardized supervision signals. In the following, we specifically detail the data construction strategies for tasks that necessitated specialized algorithmic generation or heuristic filtering, as opposed to direct annotation usage.

¹https://huggingface.co/SamLowe/roberta-base-go_emotions

²<https://saifmohammad.com/WebPages/nrc-vad.html>

Coordinate System Standardization To ensure consistency across egocentric and allocentric reasoning tasks, we transformed all spatial annotations into a unified Ego-Centric Cartesian Coordinate System. The ego vehicle’s centroid is defined as the origin $(0, 0)$. Following standard autonomous driving conventions, the positive X-axis points to the vehicle’s forward direction, and the Y-axis represents the lateral dimension. We converted the raw pixel coordinates from the Bird’s-Eye View (BEV) maps into metric coordinates using the dataset’s resolution (10 pixels/meter). All target locations and trajectory waypoints were transformed into this local frame relative to the ego vehicle’s position at the current timestamp.

Egocentric Spatial Grounding We utilized the 2D bounding box annotations provided by the dataset for the referred object in the frontal camera view. The bounding box coordinates $(x_{min}, y_{min}, x_{max}, y_{max})$ were normalized relative to the image dimensions to serve as the regression target for the visual grounding token `<ego>`.

Egocentric Spatial Relation Since the dataset does not provide explicit categorical spatial labels, we algorithmically generated these labels to train the model’s spatial reasoning. To acquire robust 3D positional information from the 2D frontal images, we utilized the standard 3D object detection results (FCOS3D [62]) provided by the Talk2Car benchmark. We first filtered these detections based on a high confidence threshold to ensure reliability. Furthermore, to eliminate referential ambiguity, where multiple objects of the same class (e.g., multiple “cars”) co-exist, making the spatial relation ill-defined without complex descriptors, we excluded samples containing duplicate object classes. For the remaining unambiguous targets, we computed the geometric angle θ of the target’s centroid relative to the ego vehicle in the metric allocentric space and discretized it into five distinct classes (Directly Ahead, Front-Left, Front-Right, Left, Right).

Egocentric Depth Estimation To supervise 3D perception recovery, we employed the same detection-based data construction strategy. Using the high-confidence (> 0.3), non-ambiguous 3D detections described above, we computed the ground truth depth as the Euclidean distance between the ego vehicle’s centroid and the target object’s predicted 3D centroid. This scalar value serves as the regression target, ensuring the model learns to extract depth cues for specific, unambiguous objects from the 2D frontal view.

Allocentric Target Location Estimation For the allocentric localization task, we generated specialized visual inputs by rendering the geometric annotations onto the raw BEV semantic maps. Specifically, we superimposed the polygons of the ego vehicle (colored red) and the referred target object (colored yellow) onto the map image using their ground-truth annotations. This visual augmentation provides explicit cues for the model to learn the mapping between visual map features and metric locations. The supervision target is defined as the metric coordinates (x, y) of the target object’s centroid relative to the ego vehicle, transformed into the unified coordinate system described above.

B. Experimental Setups

B.1. Datasets

We evaluate E3AD across four challenging real-world benchmarks: Talk2Car [14], DrivePilot [19], MoCAD [34], and Talk2Car-Trajectory [15]. Specifically:

Talk2Car. Talk2Car is built on top of nuScenes [3] and provides 11,959 natural-language commands over 9,217 urban driving images captured in Singapore and Boston. Commands average 11 words and frequently express multi-step, relational reasoning. A linguistic breakdown shows rich syntactic variability (avg. 2.32 nouns, 2.29 verbs, 0.62 adjectives per command), and each video segment is paired with ~ 14 commands, providing strong multimodal grounding supervision. We use the official split: 8,349 training, 1,163 validation, and 2,447 testing commands.

DrivePilot. DrivePilot is a new dataset that supports open-domain grounding in complex scenes. It leverages Qwen2-VL under regularized prompts to generate structured semantic annotations describing weather, scene context, traffic participants, emotional cues, and interaction patterns. Each sample contains a natural-language instruction, front-view and BEV images, LLM-generated descriptions, and precise target-object localization. DrivePilot is designed to challenge fine-grained referent disambiguation and command comprehension in realistic, congested urban scenes.

MoCAD. MoCAD originates from Macau’s Level-4 autonomous bus deployment and covers over 300 hours of real-world driving. It includes data from a 5 km campus route, an extended 25 km urban corridor, and dense traffic scenarios under varying weather and lighting conditions. The dataset contains $\sim 13k$ images and $\sim 40k$ annotated objects with commands averaging 12.5 words. Its right-hand-driving configuration differs from many datasets, making MoCAD a valuable benchmark for domain shift, layout adaptation, and cross-cultural grounding robustness.

Talk2Car-Trajectory. Talk2Car-Trajectory augments Talk2Car with multiple human-annotated feasible trajectories for each command. Following the cropping protocol in [15], samples whose referred object falls outside the 120×80 m BEV region are removed. The final Talk2Car-Trajectory splits contain 8,301 training commands (mean path length 28.37 m, with 99.55% of samples annotated with three trajectories), 1,149 validation commands (mean path length 27.98 m, 99.31% with three trajectories), and 2,439 test commands (mean path length 28.41 m, 98.81% with three trajectories). Each command is paired with multiple feasible human-annotated paths, enabling evaluation under diverse ground-truth futures. We adopt this dataset to evaluate end-to-end grounding and navigation quality under multiple ground-truth futures.

B.2. Evaluation Metrics

This section provides the formal definitions of the metrics used in OD-E2E AD, including visual grounding, spatial reasoning, and trajectory planning. Specifically:

Intersection-over-Union (IoU). For the visual grounding evaluation, we evaluate grounding using Intersection-over-Union (IoU). Given the predicted bounding box \hat{b} and the ground-truth box b , the IoU can be formally defined as:

$$\text{IoU}_{50}(\hat{b}, b) = \frac{\text{Area}(\hat{b} \cap b)}{\text{Area}(\hat{b} \cup b)}. \quad (6)$$

A prediction is considered correct if $\text{IoU} > 0.5$, following the ECCV Commands 4 Autonomous Vehicles protocol.

For spatial reasoning, we report Mean Absolute Error (MAE) and IoU for spatial reasoning tasks. Formally, **Target Location MAE.** Let $p \in \mathbb{R}^2$ denote the ground-truth target location and \hat{p} denotes the estimated target location, and the target location MAE is defined as follows:

$$\text{MAE}_{\text{loc}} = \|\hat{p} - p\|_2. \quad (7)$$

Depth Estimation MAE. Given predicted depth \hat{d} and ground truth d , the depth estimation MAE are defined as:

$$\text{MAE}_{\text{depth}} = |\hat{d} - d|. \quad (8)$$

Accuracy. The accuracy within g meters (PA_g) is defined:

$$\text{PA}_g = \mathbb{I}(\|\hat{p} - p\|_2 \leq g). \quad (9)$$

For trajectory planning, let the predicted trajectory be $\hat{\tau} = \{\hat{p}_1, \dots, \hat{p}_{N_p}\}$ and the ground-truth trajectory be $\tau = \{p_1, \dots, p_{N_p}\}$, the planning metrics are defined as follows:

Average Displacement Error (ADE).

$$\text{ADE}(\hat{\tau}, \tau) = \frac{1}{N_p} \sum_{i=1}^{N_p} \|\hat{p}_i - p_i\|_2. \quad (10)$$

Final Displacement Error (FDE).

$$\text{FDE}(\hat{\tau}, \tau) = \|\hat{p}_{N_p} - p_{N_p}\|_2. \quad (11)$$

Discrete Fréchet Distance. Let $\hat{\tau} = [\hat{p}_1, \dots, \hat{p}_{N_p}]$ and $\tau = [p_1, \dots, p_{N_p}]$, the discrete Fréchet distance is defined:

$$\text{Fréchet}(\hat{\tau}, \tau) = \min_{\alpha, \beta} \max_t \|\hat{p}_{\alpha(t)} - p_{\beta(t)}\|_2, \quad (12)$$

where α, β are monotone reparameterizations.

Dynamic Time Warping (DTW). The DTW is defined as:

$$\text{DTW}(\hat{\tau}, \tau) = \min_{\pi} \sum_{(i,j) \in \pi} \|\hat{p}_i - p_j\|_2, \quad (13)$$

where π is a warping path preserving temporal order.

Symmetric Segment-Path Distance (SSPD). For path-to-segment distance $\text{SPD}(a, b)$:

$$\text{SSPD}(\hat{\tau}, \tau) = \frac{1}{2} [\text{SPD}(\hat{\tau}, \tau) + \text{SPD}(\tau, \hat{\tau})]. \quad (14)$$

B.3. Decoder Setups

For the decoder, we select the best-performing baseline, PTPC, as the trajectory generator. We first replace the native object detection module of PTPC with the visual grounding results generated by our model, utilizing our predicted bounding box as the definitive target prior. Furthermore, we incorporate our predicted coarse trajectory as a spatial guidance signal; specifically, we encode the coarse waypoints into an additional layout tensor layer, which is concatenated with the original environmental layout features during training. This integration provides a robust spatial prior that constrains the search space for fine-grained physical refinement. Notably, this output format, comprising explicit 2D waypoints and grounded coordinates, is geometric and model-agnostic, ensuring that our framework is not limited to PTPC but can be seamlessly adapted to various trajectory decoders that accept spatial priors or goal-conditioned inputs.

C. User Study

To comprehensively evaluate the human-centric capabilities of E3AD, we conducted a user study involving $N = 217$ participants. This section details the participant demographics, experimental design, and quantitative analysis methods used to generate the results presented in Figure 7 of the main text.

C.1. Participant Demographics

We recruited a diverse group of participants to ensure the evaluation reflects a wide range of user perspectives. The demographic distribution (Figure A2) covers various age groups, genders, and driving experience levels:

- **Age Groups:** Participants were categorized into four brackets: 18–25, 26–35, 36–50, and 50+. This stratification allows us to analyze acceptance levels across different generational cohorts.
- **Gender Balance:** The study included Male, Female, and Non-binary participants to minimize gender bias in the evaluation of driving comfort and safety perception.
- **Driving Experience:** We classified participants into *Beginner*, *Intermediate*, and *Expert* levels. This distinction is crucial as experienced drivers typically prioritize safety and compliance, while novices may prioritize comfort and perceived intelligence.

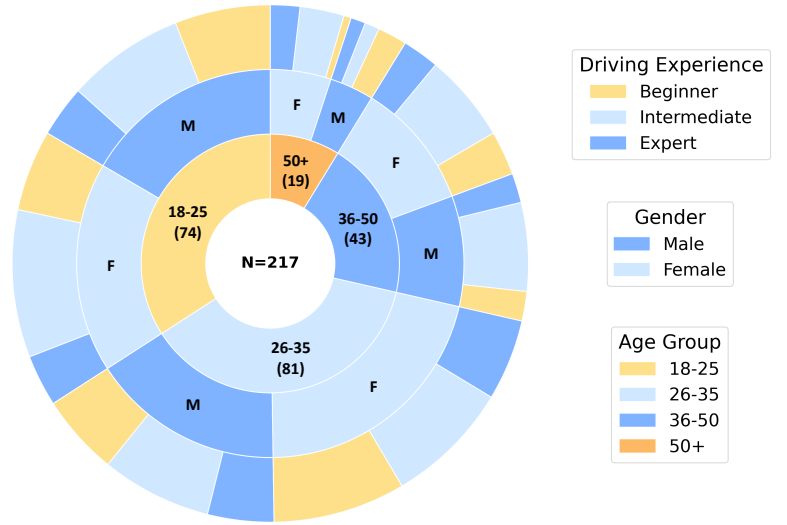


Figure A2. Demographic breakdown of the 217 participants in the user study. The sunburst chart illustrates the hierarchical distribution across three dimensions: **Age Group** (Inner Ring), **Gender** (Middle Ring), and **Driving Experience** (Outer Ring).

C.2. Experimental Design and Baselines

Participants were presented with anonymized video clips of driving scenarios. For each scenario, they viewed the trajectory and textual feedback generated by five distinct systems: (1) E3AD (Ours), (2) CAVG, (3) FSDrive-FT, (4) Qwen2.5-VL-72B, (5) Qwen3-VL-8B. The model names were hidden to prevent brand bias (Blind Test). Participants were asked to rank the five systems from 1 (Best) to 5 (Worst) across five specific dimensions.

C.3. Evaluation Metrics

The ranking task was conducted along the following axes:

- **Command Compliance:** How accurately the vehicle executed the semantic instruction (e.g., “Park behind the red car”).
- **Emotion Alignment:** How well the driving style (speed, aggressiveness) matched the emotional tone of the command (e.g., urgency vs. caution).
- **Safety:** The perceived physical safety of the maneuver (e.g., distance from obstacles).
- **Comfort:** The smoothness of the trajectory and the reassuring nature of the verbal feedback.
- **Preference:** The user’s overall subjective preference for the system as an autonomous driving assistant.

C.4. Analysis Methodology

To quantify the rankings, we converted the ordinal rank data into numerical scores. A Rank-1 vote (Best) was assigned 5 points, scaling down to a Rank-5 vote (Worst) assigned 1 point.

Rank-1 Distribution (Polar Plot) The polar plot in Figure 7 (Right) visualizes the count of Rank-1 votes received by each model across the five dimensions. E3AD (Yellow) dominates the outer perimeter, indicating it was most frequently chosen as the top-performing model, particularly in *Emotion* and *Compliance*.

Age Group Analysis (Bar Charts) The bar charts in Figure 7 (Left) display the mean score (1–5 scale) achieved by E3AD across different age groups. The error bars represent the standard deviation. The results demonstrate robust performance consistency:

- **Younger Cohorts (18-35):** Show high preference for *Emotion* and *Compliance*, indicating a desire for responsive and interactive agents.
- **Older Cohorts (36-50+):** While generally more critical of automated systems, they assigned high scores to E3AD’s *Safety* and *Comfort*, validating the effectiveness of our emotion-aware planning in building trust.

D. Supplementary Results

D.1. Qualitative Results

We provide additional qualitative results in Figure A3 to further demonstrate the robustness of E3AD across diverse driving scenarios, ranging from lane changing and turning to parking and car following. In each case, the model successfully grounds the target object referenced in the command and generates a feasible trajectory. Crucially, the visualized `<EmoThink>` and `<Feedback>` outputs illustrate the model’s ability to interpret fine-grained emotional cues, such as urgency, caution, or confidence, from the natural language command and generate human-centric responses that are tonally aligned with the passenger’s state.

D.2. Effects of Emotion-Action Alignments

Training Dynamics and Convergence. Before evaluating the generated trajectories, we first verify the optimization stability of the DPO process. As illustrated in Figure A4, the training exhibits two critical trends. First, the NLL Loss (**red curve**) rapidly decreases and stabilizes, indicating that the policy is successfully modeling the probability distribution of the ground-truth trajectories without mode collapse. Second, and crucially, the Reward Margin (**blue curve**), defined as the log-probability gap $\log p_\theta(\tau^{(i)}|C^{(i)}) - \log p_\theta(\tilde{\tau}_{k-}^{(i)}|C^{(i)})$, shows a consistent upward trend. This increasing margin confirms that the model is effectively learning to distinguish between the optimal ground-truth $\tau^{(i)}$ and the emotion-shifted negative samples $\tilde{\tau}_{k-}^{(i)}$ (constructed in Eq. 4), assigning higher likelihoods to the alignment-consistent trajectories. The simultaneous convergence of both metrics validates that the optimization objective in Eq. 5 has been effectively minimized.

To quantitatively evaluate whether the generated trajectories reflect the intended emotional semantics and physical realism, we analyze the geometric properties of the trajectories. Let a generated trajectory be denoted as $\hat{\tau} = \{\hat{p}_1, \dots, \hat{p}_{N_p}\}$, where $\hat{p}_i \in \mathbb{R}^2$ represents the spatial coordinates at step i , and N_p is the horizon length.

D.2.1. Metric Definitions

We adopt four geometric metrics to characterize the motion patterns. While *Straightness* measures global efficiency, we introduce a deviation-based *Sinuosity* to explicitly capture local instability (jitter), which is critical for evaluating trajectory generation.

Straightness: Defined as the ratio of the Euclidean distance between the start and end points to the total path length. It indicates global transport efficiency:

$$\mathcal{M}_{\text{str}} = \frac{\|\hat{p}_{N_p} - \hat{p}_1\|_2}{\sum_{i=1}^{N_p-1} \|\hat{p}_{i+1} - \hat{p}_i\|_2} \quad (15)$$

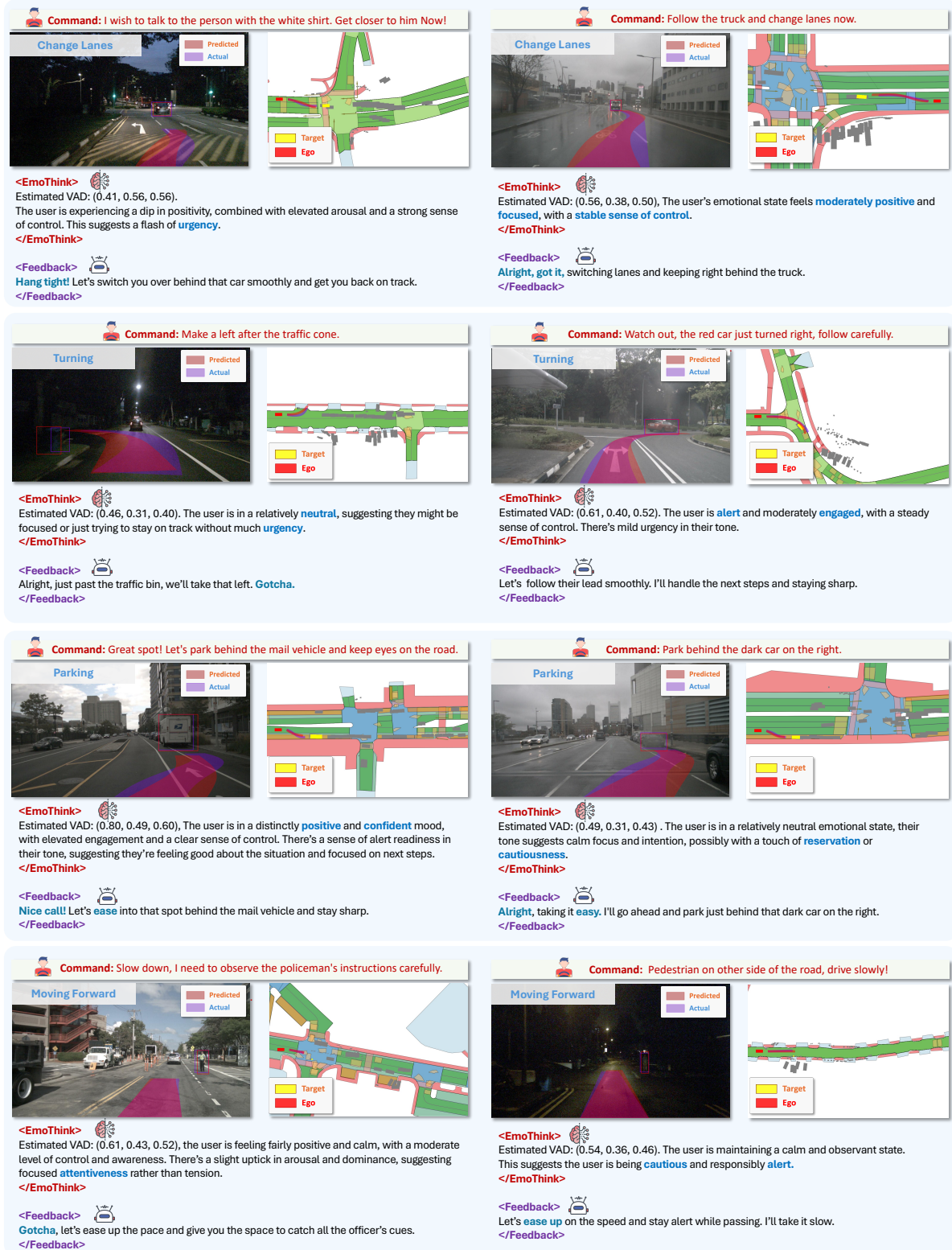


Figure A3. Additional qualitative examples of E3AD across different driving maneuvers (Change Lanes, Turning, Parking, Moving Forward). For each sample, we display the input command, the egocentric view with visual grounding, and the allocentric map with the predicted trajectory. The outputs include the estimated VAD scores, the chain-of-thought emotional analysis (<EmoThink>), and the generated verbal response (<Feedback>), highlighting how the system adapts its interaction style to the detected emotional intent (e.g., responding with “Hang tight!” for urgent commands versus “Taking it easy” for cautious ones).



Figure A4. **DPO Training Dynamics.** The **red curve** denotes the **NLL Loss**, reflecting policy optimization, while the **blue curve** tracks the **Reward Margin** (the log-probability gap between preferred and rejected trajectories). The decrease in loss and increase in margin demonstrate successful convergence and preference learning.

Table A1. **Quantitative Evaluation of DPO Efficacy.** **Panel A** assesses *emotion alignment*, showing that DPO recovers the correct arousal-response patterns (physical laws) observed in Ground Truth. **Panel B** evaluates *physical structural alignment*, demonstrating that DPO significantly enhances the geometric fidelity of the generated trajectories relative to Ground Truth.

Metric	Straightness	Mean Turn	Angle Var.	Sinuosity
Panel A: Arousal Alignment Error (Target: Match GT)				
GT Correlation (Ref)	0.161	−0.163	−0.155	−0.158
w/o DPO	−0.029	0.023	0.030	0.033
Δ Abs. Error ↓	0.190	0.186	0.185	0.191
w/ DPO	0.167	−0.183	−0.158	−0.166
Δ Abs. Error ↓	0.006	0.020	0.003	0.008
Error Reduction ↑	96.8%	89.2%	98.4%	95.8%
Panel B: Physical Alignment Quality (Target: High Correlation with GT)				
w/o DPO	0.579	0.476	0.462	0.576
w/ DPO	0.633	0.519	0.490	0.629
Improvement ↑	+9.3%	+9.0%	+6.1%	+9.2%

Mean Turn: The average absolute change in heading angle, reflecting the tortuosity of the path. Let θ_i be the heading angle at step i , then:

$$\mathcal{M}_{\text{turn}} = \frac{1}{N_p - 2} \sum_{i=1}^{N_p-2} |\theta_{i+1} - \theta_i| \quad (16)$$

Angle Variance: Measures the smoothness and consistency of directional changes. Let δ_i be the turning angle at step i , defined as the angular difference between consecutive heading vectors (adjusted to $(-\pi, \pi]$). The variance is computed as:

$$\mathcal{M}_{\text{var}} = \frac{1}{N_p - 2} \sum_{i=1}^{N_p-2} (\delta_i - \bar{\delta})^2 \quad (17)$$

where $\bar{\delta}$ is the mean turning angle. High variance indicates a trajectory with erratic or jerky steering patterns.

Sinuosity (Lateral Deviation): Unlike the standard length-based definition (which is the reciprocal of straightness), we define Sinuosity as the **Mean Lateral Deviation** to capture path oscillation. It is calculated as the average perpendicular distance of all points from the ideal straight line connecting the start (\hat{p}_1) and end (\hat{p}_{N_p}):

$$\mathcal{M}_{\text{sin}} = \frac{1}{N_p} \sum_{i=1}^{N_p} \frac{|(\hat{p}_{N_p} - \hat{p}_1) \times (\hat{p}_i - \hat{p}_1)|}{\|\hat{p}_{N_p} - \hat{p}_1\|_2} \quad (18)$$

where \times denotes the 2D cross-product (determinant). This metric is sensitive to the high-frequency jitter often observed in unaligned generative models.

D.2.2. Quantitative Analysis

We evaluate the efficacy of Direct Preference Optimization (DPO) from two perspectives: *Semantic Alignment* (consistency with emotional laws) and *Physical Alignment* (geometric fidelity to ground truth). The results are summarized in Table A1 (Panel A and B).

Emotion Alignment (Panel A). We compute the Spearman rank correlation (ρ) between the input *Arousal* value and the extracted trajectory features. In the Ground Truth (GT) dataset, Arousal is negatively correlated with turning behaviors (e.g., $\rho_{\text{turn}} = -0.163$), implying that high-arousal movement tends to be more direct. As shown in Panel A, the baseline model (w/o DPO) exhibits a *sign error*, incorrectly predicting a positive correlation ($\rho = 0.023$) and failing to capture the underlying physical law. In contrast, the DPO-aligned model successfully recovers the correct negative correlation ($\rho = -0.183$), reducing the alignment error by 89.2% to 98.4% across all metrics. This confirms that DPO effectively injects the correct emotion-action constraints into the policy.

Physical Structural Alignment (Panel B). We further calculate the Spearman correlation between the geometric features of the generated trajectories $\hat{\tau}$ and the paired ground truth τ . Higher correlation indicates better preservation of the realistic geometric structure. As shown in Panel B, DPO consistently improves the structural fidelity. Notably, for the *Sinuosity* metric defined in Eq. (12), DPO achieves a 9.2% improvement ($0.576 \rightarrow 0.629$). This significant gain suggests that the DPO-trained model effectively suppresses unrealistic trajectory jitter and oscillation, resulting in smoother and more human-like motion paths compared to the baseline.

E. Prompts Design

Modality Pretraining During the initial pretraining stage, we utilize discrete, task-specific prompts to equip the model with foundational spatial and emotional capabilities. As illustrated in the left and top-right panels of Figure A5, these include:

- **Egocentric Spatial Grounding:** The model is prompted with the frontal view token `<ego>` to output the 2D bounding box of the target. This trains the model’s ability to visually align linguistic semantics with the immediate first-person perceptual field, which is essential for short-horizon interaction.
- **Egocentric Spatial Relation:** To mimic human-like spatial cognition, this prompt asks the model to classify the target’s relative position (e.g., “Front-Left”) rather than just regressing coordinates. This facilitates a more robust understanding of directionality and relative bearings in the ego-coordinate system.
- **Egocentric Depth Estimation:** This task prompts the model to regress the Euclidean distance to the target. It explicitly supervises the vision encoder to recover 3D metric depth from 2D frontal images, a critical capability for maintaining safety margins and longitudinal control.
- **Allocentric Target Location Estimation:** Using the allocentric token `<allo_ego_target>`, the model estimates target coordinates in the map frame. This task aligns the visual representation with a world-centered “cognitive map,” enabling the agent to resolve occlusions and understand global scene topology.
- **Waypoint Planning:** We employ separate prompts for both Egocentric and Allocentric views to predict the future waypoints. By enforcing the model to derive the same trajectory from distinct visual perspectives, we ensure that the planning policy is grounded in both immediate perceptual cues (Egocentric) and global structural constraints (Allocentric), fostering robust spatial representations that are consistent across views.
- **Emotion Modeling:** This text-only prompt instructs the model to map the command into the continuous Valence, Arousal, and Dominance (VAD) space. This acts as a cognitive prior, allowing the system to distinguish the urgency and tone of the request before planning.

Joint Fine-tuning In the second stage, we employ a unified prompt template to enable Emotion-aware Chain-of-Thought (CoT) reasoning. As shown in the “Joint Fine-tuning” panel of Figure A5, the input sequence concatenates the synchronized visual tokens (`<allo>` and `<ego>`) with the user command. The prompt explicitly instructs the model to perform three tasks in sequence: (1) analyze the VAD values, (2) visually ground the target in the frontal view, and (3) predict the future waypoints. This autoregressive structure ensures that the final trajectory planning is conditioned on both the emotional interpretation and spatial grounding results.

Emotion-Action Alignment To align the model’s behavior with human emotional intent, we utilize the Direct Preference Optimization (DPO) prompt template. As depicted in the “Emotion-Action Alignment” panel, this prompt presents the visual context and command, soliciting a trajectory prediction. During training, this is structured as a preference pair: the *Preferred* output contains the ground-truth trajectory corresponding to the original command, while the *Rejected* output contains a trajectory generated from an emotion-augmented “negative” command (e.g., a trajectory that ignores urgency or caution). This guides the model to prefer actions that are consistent with the emotional tone of the instruction.

Inference During the inference phase, E3AD utilizes the same prompt structure as the Joint Fine-tuning stage. The system receives the multi-view image tokens and the natural language command as input. It then generates the full response sequence end-to-end: first estimating the VAD emotion state, then locating the target object, and finally planning the waypoints. This unified prompting strategy allows the model to dynamically adapt its planning strategy based on the inferred emotional urgency and spatial context without requiring separate task triggers.



Figure A5. Overview of the prompt templates utilized in the E3AD framework across different training stages. The figure details the specific instructions and input/output formats for tasks including spatial grounding, depth estimation, emotion modeling, and trajectory planning. Note that the text elements marked in blue (i.e., `<ego>`, `<allo>`, `<allo_ego_target>`, `<allo_ego>`) represent the special visual tokens corresponding to the egocentric view, allocentric view, and the allocentric view with the target object highlighted, respectively.